LETTER Communicated by Sebastian Seung and Miguel Nicolelis

Temporal-Code to Rate-Code Conversion by Neuronal Phase-Locked Loops

Ehud Ahissar
Department of Neurobiology, Weizmann Institute of Science, Rehovot 76100, Israel

Peripheral sensory activity follows the temporal structure of input signals. Central sensory processing uses also rate coding, and motor outputs appear to be primarily encoded by rate. I propose here a simple, efficient structure, converting temporal coding to rate coding by neuronal phase-locked loops (PLL). The simplest form of a PLL includes a phase detector (that is, a neuronal-plausible version of an ideal coincidence detector) and a controllable local oscillator that are connected in a negative feedback loop. The phase detector compares the firing times of the local oscillator and the input and provides an output whose firing rate is monotonically related to the time difference. The output rate is fed back to the local oscillator and forces it to phase-lock to the input. Every temporal interval at the input is associated with a specific pair of output rate and time difference values; the higher the output rate, the further the local oscillator is driven from its intrinsic frequency. Sequences of input intervals, which by definition encode input information, are thus represented by sequences of firing rates at the PLL's output. The most plausible implementation of PLL circuits is by thalamocortical loops in which populations of thalamic "relay" neurons function as phase detectors that compare the timings of cortical oscillators and sensory signals. The output in this case is encoded by the thalamic population rate. This article presents and analyzes the algorithmic and the implementation levels of the proposed PLL model and describes the implementation of the PLL model to the primate tactile system.

1 Introduction

The distinction between rate and temporal coding is not always clear (Theunissen & Miller, 1995). For example, temporal coding is sometimes regarded as rate coding with a fine time resolution. In this article, temporal coding will refer to coding in which the exact time of every spike is informative. Rate coding will be associated here with a temporal window, the rate bin, within which the exact temporal information is not informative and the information is carried by the average firing rate over the entire temporal window. The rate bin is usually determined by the integration times of the readout mechanisms. A rate encoded signal can thus be described by a series of numbers, each of which represents the average firing rate in a

single rate bin (see appendix A.1). Fluctuations in the average firing rate of a neuron over different rate bins are considered here as fluctuations of rate-encoded information, and not as temporal coding, as has been considered previously (Richmond & Optican, 1987). A temporally encoded signal is described by a series of numbers, each of which represents either the timing of a single spike or a single interspike interval (ISI; see appendix A.1). The information contained in the spiking times can be presented in different ways; two of them are depicted in Figure 1: $M(n)$ describes the deviations of the actual train from an imaginary, ideally periodic, "carrier" train and $I(n)$ describes the ISIs. Figure 1 also demonstrates the distinction between temporal and rate coding; the spike train in this example carries a significant amount of information if a temporal coding is assumed (see Figure 1a), but almost no information if a rate coding with a particular rate bin is assumed (see Figure 1b). Practically, this distinction is important for reading out the information of the spike train. A readout mechanism based on rate will lose more and more information as its integration time increases. To read out temporally encoded information, a rate-based mechanism needs to employ integration times shorter than half of the input temporal resolution, an implementation that is both nonefficient and, with fine input resolution, not practical for neurons. The other alternative is to utilize preprocessing by time-sensitive mechanisms—mechanisms that produce populations of spikes, where the number of spikes in a population directly represents the ISI at the input and the exact times of these output spikes is not important.

Another important distinction is between peripheral and central temporal encodings (Perkel & Bullock, 1968). When a stimulus is temporally encoded at the periphery, the peripheral ISIs directly describe stimulus features such as spatial periods (Darian-Smith & Oke, 1980) whereas when stimuli are temporally encoded centrally, the centrally generated temporal structures are usually not directly related to the stimulus (Engel, Konig, Kreiter, Schillen, & Singer, 1992; Abeles, Bergman, Margalit, & Vaadia, 1993). This article deals with central decoding of peripherally generated temporal encodings. Using the term *decoding* in neuronal contexts should not imply that the original signals are reconstructed, but rather that the encoded information is extracted (Perkel & Bullock, 1968).

In mammals, sensory information is encoded by both rate and temporal coding (Sejnowski, 1995; Carr, 1993; Middlebrooks & Green, 1991; Wang, Merzenich, Beitel, & Schreiner, 1995; Johansson & Vallbo, 1983; Berkley, 1978). Whereas spatial static information is usually encoded by rate, dynamic information, generated during movements of either the stimulus or the sensory organ, is encoded also by temporal cues (see, for example, encoding of spatial intervals by ISIs of tactile [Darian-Smith & Oke, 1980] and visual [Shadlen & Newsome, 1994] neurons). In contrast, motor control is assumed to utilize rate coding predominantly (Georgopoulos, 1986; Fetz, 1993; Wise, 1993), even at the early stage of motor planning (Boussaoud & Wise, 1993). Thus, information carried by the sensory temporal

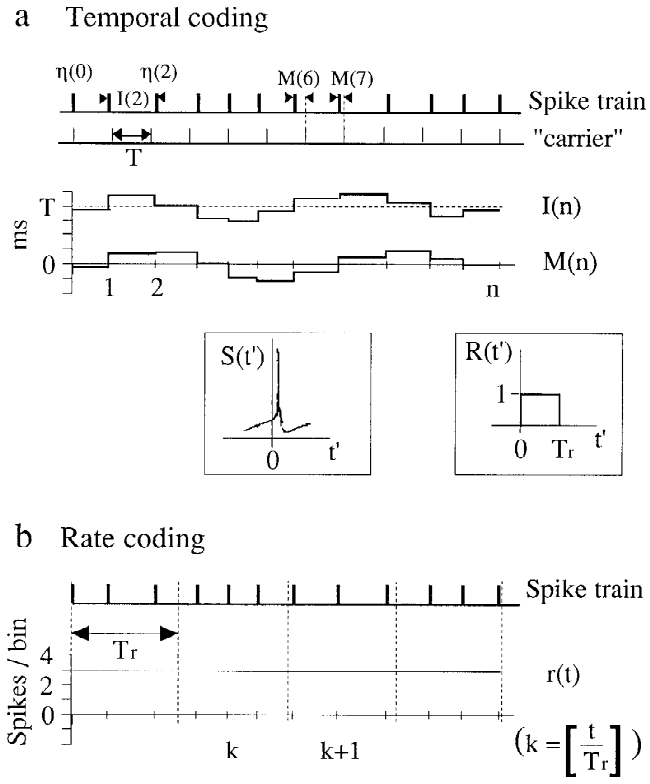

Figure 1: Encoding by spike trains. (a) Temporal encoding. Two possible presentations of the information contained in the spiking times: a series of ISIs [$I(n)$] and a series of absolute modulations [$M(n)$]. $M(n)$ is the difference between the actual timing of the nth spike and the timing expected by an imaginary, ideally periodic, "carrier" train that has the same average periodicity and no modulation (see appendix A1). (b) Rate encoding. The spike train is divided into several rate bins (four in this case), and the total number of spikes in each bin determines the value of the rate function $r(t)$ for that bin. Insets: $S(t')$, a spike triggered at $t' = 0$; $R(t')$, a step function with a unity gain and a duration of a rate bin, T_r.

components is probably translated, by neuronal circuits in the brain, to rate-encoded signals that are "readable" by the motor system. If such a translation occurs early in a sensory pathway, the translation would also facilitate integration of temporally encoded information with other, rate-encoded sensory information. This necessity for translation was elegantly demonstrated by Mountcastle and his colleagues (Talbot, Darian-Smith, Ko-

rnhuber, & Mountcastle, 1968; Mountcastle, 1993) over the past few decades.

A mechanism that utilizes neuronal delay lines to transform temporal coding to rate coding has been suggested by Jeffress (1948). Such delay lines exist in the electric sensory system of electric fishes and in the subcortical auditory systems of birds and mammals (reviewed in Carr, 1993). These delay lines are probably utilized to decode temporal disparities, which in the submillisecond and low millisecond ranges can determine interaural time differences and echo delays, respectively. As the delay increases above a few hundred microseconds, implementations of delay lines require multiple neuronal elements, and the accuracy decreases (Carr, 1993). A mechanism that uses synaptic time constants appears more suitable to decode temporally encoded information in the millisecond range (Buanomuno & Merzenich, 1995). Both of these mechanisms describe "passive," open-loop decoding schemes that are based on classification of different ISIs according to their interaction with predetermined neuronal temporal features. In this article, I suggest an "active," closed-loop decoding mechanism, which dynamically adapts its working parameters to match the incoming signal. This phase-locked loop (PLL) model is based on a local oscillator "measuring" the instantaneous temporal period of the input by comparing it to its own period. During decoding, the local oscillator updates its period according to the result of the comparison, such that it remains tuned to the changing input. The PLL is a well-known mechanism in electrical engineering where it is often used for the decoding of phase-modulated signals. The algorithm presented here was adopted from that of continuous-time electronic PLLs (Gardner, 1979) and modified to fit discrete-time neuronal PLLs. This approach uses a small neuronal network as a PLL, unlike a previous approach that described a single-neuron as a PLL (Hoppensteadt, 1986).

Neuronal PLLs appear suitable to decode temporally encoded information in the range of a few to a few hundred milliseconds. However, decoding by a single neuronal PLL is usually limited to phase modulations that are in the order of its intrinsic period. Thus, decoding in different frequency ranges requires different PLL circuits, and decoding of large modulations requires an ensemble of several PLLs. In this article, the mechanism of a single PLL is described in detail, whereas only the principles of operation are described for the postulated ensemble.

Depending on the parameters of a stimulus, sensory firing could engage different temporal forms. For example, the peripheral tactile response to a moving grating can be one spike per bar or a burst of a variable length per bar (Darian-Smith & Oke, 1980; Morley and Goodwin, 1987). For clarity, simple temporal forms will be assumed here. Sensory firing with bursts does not affect the principles of decoding described here (S. Serulnik and E. Ahissar, unpublished observations), although it affects the decoding details.

2 The PLL Model

2.1 The PLL Algorithm. The simplest version of a first-order PLL (Gardner, 1979) is adopted here. A first-order neuronal PLL is composed of two elements (see Figure 2a): a phase detector (PD) and a rate-controlled oscillator (RCO). The RCO is a local oscillator whose output frequency, and thus the timing of its output spikes, is controlled by the firing rate of its input. If the input is zero, the RCO will fire at its intrinsic frequency. The more excitatory the input, the higher the RCO's output frequency, and the more inhibitory the input, the lower is the RCO's frequency. The PD compares the phase—the time of arrival—of each of the spikes of a repetitive input against the phase of the RCO spikes and produces an output that is a "measure" of (i.e., its firing rate is proportional to) that phase difference. The RCO can be regarded as a rate-to-temporal code converter and the PD as a temporal-to-rate converter. The PD's output (R_d) is fed into the RCO's input and changes the RCO's firing phase in the direction that will cancel the phase difference (in fact, cancel any deviation from some constant phase difference), establishing a negative feedback loop (see section A.2). Note that in the following description *phase difference* and *temporal difference* are interchangeable terms, both expressed in time units.

The PLL is considered *locked* when the RCO's instantaneous frequency equals the input's instantaneous frequency. The phase difference, in the *locked* state, depends on the difference between the input frequency and the RCO's intrinsic frequency (see appendices A.3 and A.4). While locked, the RCO generates one and only one oscillation cycle for each input cycle. For simplicity, assume that a single spike represents a single cycle, even though a short burst or an ensemble of single spikes over a cell population is also possible. In the absence of noise and with ideal PLLs (see appendix A.3), the RCO's output spike train is a perfect replica of the input spike train, but with a delay of one cycle plus a constant phase shift. This is because, with ideal PLLs, any deviation of the input from the expected ISI is followed by an identical deviation of the RCO's ISI at the next cycle.

The decoding (or recoding) of the input information is based on the delayed internal replica of the input spike train. As long as the PLL is locked, the RCO's ISI has to be modulated by the same information that modulates the input ISI. Thus, the input information is represented by the rate-encoded signal that drives the RCO (see appendix A.4). This signal is the PLL's output. The same decoding mechanism can be described differently, at least for ideal PLLs: every input ISI is "stored" as the next RCO's ISI. Thus, at each cycle, an input ISI is compared with the input's previous ISI, and the change, which is the encoded information, is detected by the PD and presented as a rate-encoded signal (see appendix A.4). While the PD's (=PLL's) output is affecting the RCO at every cycle, it can be integrated over several cycles by a potential readout mechanism. The readout integration time, or rate bin, determines the maximal rate of information that can be represented inter-

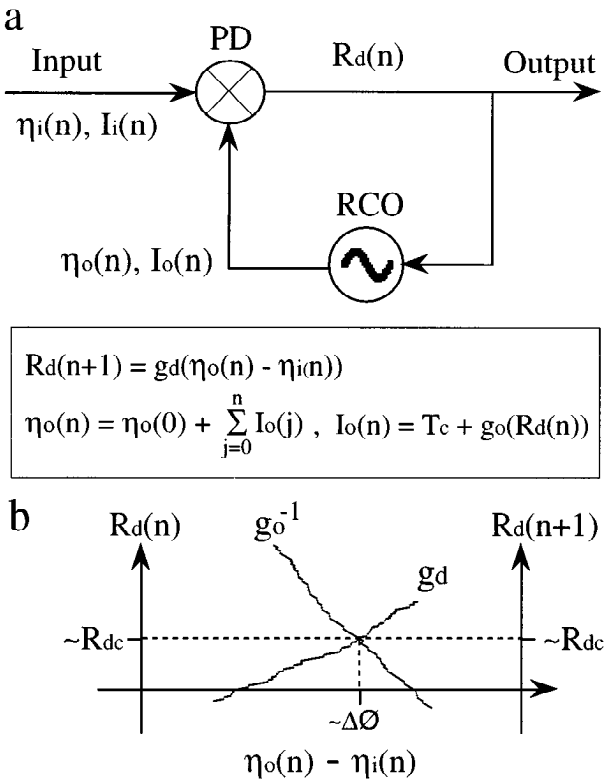

Figure 2: The first-order neuronal PLL algorithm. (a) Schematic diagram. The output of the phase detector (PD) is proportional to the difference between the timing of its two inputs. The output frequency of the rate-controlled oscillator (RCO) is modulated by the firing rate of its input (see loop equations at bottom and appendix A.2). (b) Schematic examples of transfer functions. For every I_i within the working range, $R_d(n+1)$ increases as a function of the timing difference $[\eta_o(n) - \eta_i(n)]$ and the timing difference decreases, via decrement of $I_o(n)$, and thus of $\eta_o(n)$, as a function of $R_d(n)$. The crossing (working) point is approximately (exactly for linear systems) at $(\Delta\varnothing, R_{dc})$.

nally; higher rates require shorter integration periods. Note that the phase of the input is not lost but rather preserved by the firing phase of the PLL's output, which is phase locked to the input (see, for example, Figure 6b).

Thus, the output of the PLL is a rate-encoded signal proportional to the difference between the RCO's intrinsic period and the input instantaneous ISI. This signal can be decomposed to two components: a DC component

(R_{dc}), which represents the difference between the RCO's intrinsic period and the average input ISI, and an AC component (R_{ac}), which represents the dynamic input information (see appendices A.2 and A.4). An ideal PLL should be able to track any change in the input ISI within one cycle. Practical PLLs, however, are limited in both their working ranges—the ranges of trackable input frequencies (see appendix A.2.3)—and lock-in times—the time required for moving into a new locked state. The lock-in dynamics, which is mainly determined by the loop gain (see appendix A.2.3), limits the maximal rate of change in the input frequency that a given PLL can track and decode.

PLLs of higher than first order have low-pass filters between the PD and RCO. Such filters improve the loop performance, especially in noisy conditions (Gardner, 1979; Viterbi, 1966). Low-pass filtering, also referred to as input integration, is an elementary feature of nerve cells. It is assumed that the RCO uses such filtering in its input stage. However, for simplicity, higher-order circuits will not be discussed here, since the first-order version is sufficient for code translation.

2.2 Implementations of PLLs. There are two main families of PLL implementations: excitatory PLLs (ePLLs) are those implementations in which the PD excites the RCO (see Fig. 3a, dashed lines), and inhibitory PLLs (iPLLs) are those implementations in which the PD inhibits the RCO (see Figure 3a, dotted lines). Here, only two specific implementations of these families—the AND-like and NAND-like implementations—are described in detail. Thus, ePLL will refer to an AND-like and iPLL to a NAND-like implementation, unless otherwise noted. In the following descriptions, only essential components are included, a case that probably does not occur in the brain. The described implementations should thus be regarded as building blocks that can be used separately or in combination in the brain. Accordingly, the principles of, not the exact, operation of such hypothetical PLL circuits are discussed.

The basic ePLL is a straightforward implementation of the PLL algorithm (see Figure 2) and involves two sets of neurons: the PD and RCO sets (see Figure 3a). The basic iPLL, in addition to these two sets of neurons, involves a set of inhibitory cells (INH). In both ePLL and iPLL, every component is implemented by a set of neurons similar to each other. These sets of neurons are interconnected by "diverging/converging" pathways; every cell in the projecting set sends axons to many cells in the target set, and every cell in the target set receives synapses from many cells in the projecting set. The set of RCOs of a given PLL is regarded as a set of coupled oscillators that oscillate at the same frequency. The redundancy of the RCO and INH cells has no specific role in the presented implementations beyond improving robustness. However, the efficiency of phase detection by a PD composed of a population of cells is significantly better than the efficiency of a single coincidence detector. The number of coincidence-detecting neurons that

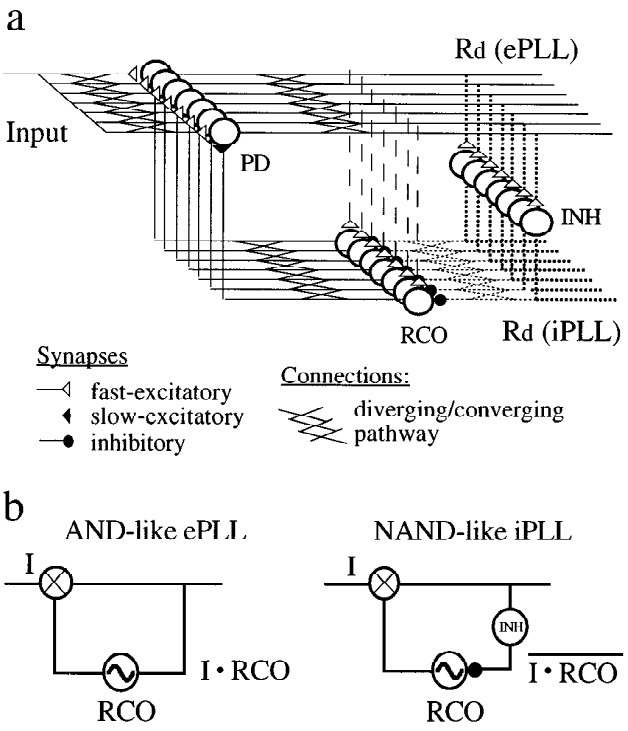

Figure 3: Possible implementations of a single PLL. (a) Connection schemes. For clarity, the width (w) was arbitrarily set at 7. Dotted lines indicate inhibitory PLL (iPLL); dashed lines, excitatory PLL (ePLL); and INH, inhibitory neurons. (b) Schematics of two possible PLL implementations where the PD operates in an AND-like manner.

compose the PD set defines the "width" (w) of a single PLL. Arbitrarily, it is assumed that the other neuronal sets (INH and RCO) have the same width. A reasonable estimation for the minimal value of w can be derived from the number of peripheral fibers activated by a "point" stimulus. In the tactile case, for example, this number is around 20 (Johansson & Vallbo, 1980).

2.2.1 Implementations of PDs. In principle, each neuron can operate as a degenerated PD. When functioning as a "coincidence detector" (Goldberg & Brown, 1969; Abeles, 1982), a cell will fire only if a certain number of its inputs will be synchronously active—that is, a single neuron detects a zero- or near-zero-phase difference among its inputs. Thus, to serve as a PD, the neuron's inputs should be predominantly organized into two groups, with

the inputs always being temporally coordinated within each group. The neuron will function as an AND-like zero-phase detector if its threshold is set such that neither of these two groups of inputs is able by itself to activate the cell, but there is a high probability that synchronous operation of both inputs will activate it. Coincidence detection, however, is not sufficient for a PD. A usable PD should have a range within which its output is a monotonic increasing or a monotonic decreasing function of the phase difference (see appendix A.2).

2.2.1.1 A single neuron AND-like PD. The PD capacity of a single neuron is due to the nonzero time constants of its inputs. If a neuron receives two major inputs, the range of delays that it will be able to resolve (i.e., its working range) will depend on the amplitude and time constants of the two inputs. For example, suppose the excitatory postsynaptic potentials (EPSPs) of both inputs, when measured at the axon hillock, exhibit short rising times, long decays, and relatively strong amplitudes (see Figure 4a). The longer the delay between the inputs—the phase difference—the shorter the period in which the membrane potential will be above threshold, and thus, the fewer the spikes that will be emitted. Thus, the output rate of a single neuronal PD is generally a monotonic decreasing function of the input phase difference.

For frequencies near 30 Hz, for example, the working range of an appropriately tuned neuron covers about half a cycle (see appendix A.5), which is satisfactory for a PD (Gardner, 1979). However, the refractoriness of a single neuron results in a poor output resolution—usually poorer than 2 ms. For example, tracking a frequency of 30 Hz with an error less than 1 Hz requires the RCO to be informed about deviations as small as 1 ms in the input spike train. A single neuron with a refractory period of 2 ms or more cannot provide this resolution. In addition, single-cell reliability is limited, and noise will significantly influence the single neuron PD's performance.

2.2.1.2 A population AND-like PD. To increase a PD's resolution, a number of single cells, say w, can be arranged in parallel such that all receive the same input, but with different delays (see Figure 4b). Let T_{wo} denote the effective width (see appendix A.5) of the RCO's output and T_{wi} the effective width of the input. The most efficient phase detection occurs with $T_{wo} = T_{wi}$. In this case, every phase difference between 0 and T_{wo} produces a different population sum (see appendix A.1) at the PD's output. Since the population sum is directly related to the overlap period, this dependency is monotonic. If the input delays are generated by constant and reliable delay lines, the phase differences will be also coded by the PD's population vector (see appendix A.1). Both "sum PD" and "vector PD" are valid PD implementations.

Schematically, the two input signals to the PD can be described as square waves (see Figure 4c) whose duty cycles are determined by their effective

widths; an input will be considered as “on” at all time points in which, had the other input been considered “on,” summation of the generated EPSPs would be suprathreshold in at least one of the PD neurons. If the PD’s output is a linear function of the inputs’ overlap time, then the transfer function would take the form described in Figure 4d (see appendix A.5).

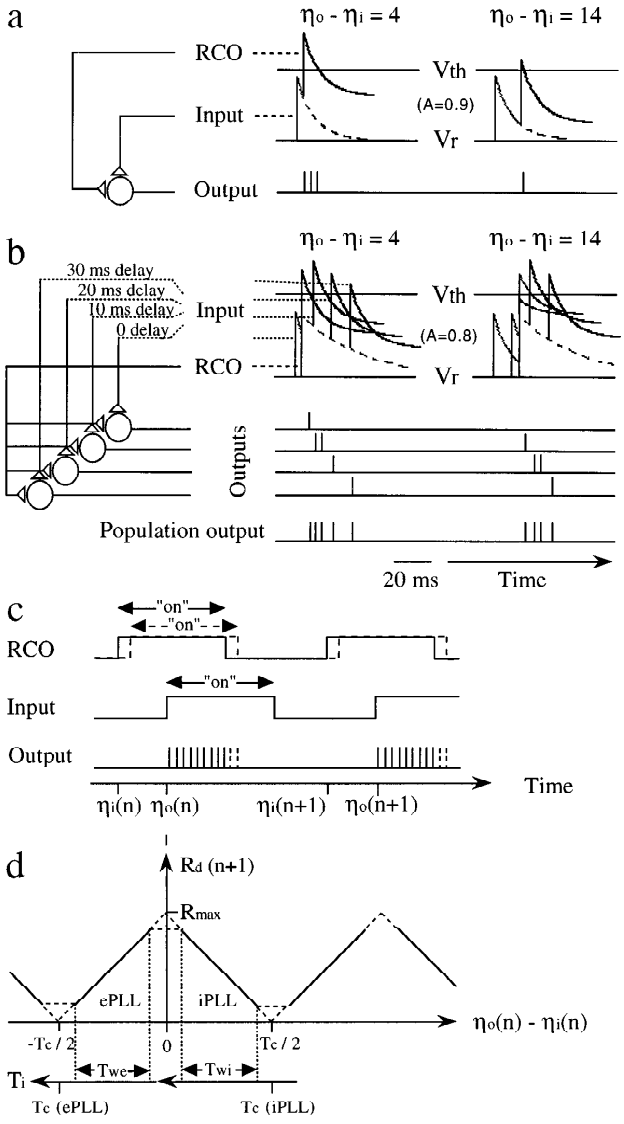

Since g_d is required to be monotonous, it is clear that a PLL can function only in limited ranges of phase differences: either within one of the increasing monotonic ranges (see Figure 4d, ePLL) or within one of the decreasing monotonic range (see Figure 4d, iPLL). In the AND-like ePLL, the RCO's output leads the input ($\eta_o - \eta_i < 0$), and in the AND-like iPLL, the RCO's output lags the input (see Figure 4d). Each of these implementations requires a different circuit to achieve the negative feedback (see appendix A.5). In the ePLL, the PD excites directly the RCO, and in the iPLL the PD excites inhibitory interneurons (INH) which, in turn, inhibit the RCO (see Figure 3 and section A.5.2). Note that the PD transfer function is periodic. Thus, large, instantaneous input modulations can move the PLL from one working range to another, producing only instantaneous tracking errors—that is, losing or "filling in" one or more input cycles.

Figure 4: *Facing page*. Implementations of neuronal AND-like PDs. (a) A single-cell PD. The two inputs, which are massive, generate two giant EPSPs with exponential decays ($A = 0.9$, $\tau = 10$ ms). More spikes are emitted when the overlapping time is larger (i.e., when there is a smaller time difference between the inputs). V_r, resting voltage; V_{th}, threshold voltage. (b) A population PD. A population of cells in which each cell receives a delayed version of the Input, each after a different delay. The RCO signal decays more slowly ($\tau = 33$ ms) than the Input and arrives simultaneously at all cells. As the time difference between the arrival of the RCO signal and the Input increases, fewer cells will be activated. (c) A schematic description of a population AND-like PD. The population signal of the Input is a pulse function, which is the "envelope" of all the delayed versions of the input, ignoring fluctuations due to EPSP shapes. At any time when both the Input and the RCO signal are "on," it is assumed that at least one of the PD cells will be activated (see section 2.2.1.2). The RCO signal is described as a pulse function, where the pulse duration is defined by the part of the RCO-driven EPSP in which adding an EPSP of the input (in any of the PD cells) will drive the membrane voltage above threshold. If the time difference between the two inputs decreases (dashed line of the RCO), the PD's output becomes stronger (two additional, dashed, spikes). (d) An example of a linear AND-like PD transfer function (g_d). The output is stronger for time delays [$\eta_o(n) - \eta_i(n)$] that have smaller absolute values (larger overlap) and monotonically decreases in response to larger time differences. The exact form of the periodic transfer function depends on the input parameters (dashed lines; see section 2.2.1.2). The working range of the iPLL includes ISIs that are longer than the intrinsic period (T_c), while the working range of the ePLL includes ISIs that are shorter than the intrinsic period.

2.2.1.3 Other PD implementations. The AND-like implementation adopted here is not the only possible one. PDs could implement an OR function, in which the PD fires when either of its two inputs is active, or an ANDNOT function, in which the PD fires only when the input is active and the RCO is silent (E. Ahissar and M. Zacksenhouse, unpublished observations). Variations of these three basic mechanisms are also possible. For example, each input can activate the PD by itself, whereas a synchronous activation augments the PD's output (an AOR operation). All of these mechanisms can be implemented in either ePLL or iPLL configurations. Since the transfer function of the RCO is probably always a decreasing one, the potential working ranges for each implementation are those in which the PD function is increasing (see appendix A.2).

2.2.2 Implementations of RCOs. Almost any single neuron can be regarded as a voltage-controlled oscillator (VCO or VCON; Hoppensteadt, 1986). However, the PLL circuit presented here requires that the RCO exhibit an explicit periodic output activity. One possible model for a neuronal intrinsic oscillator is Calvin's regenerative firing mode (Calvin, 1975). According to this model, each spike is followed by a strong afterhyperpolarization (AHP), which recovers at some rate until it reaches the threshold again, generates a new spike, and then restarts the process. The average ISI, T_o, is determined by the depth of the AHP and the average input to the neuron. Modulations of the input produce modulations of the RCO's ISI (inhibition extends $I_o(t)$, whereas excitation shortens it (Calvin, 1975; Perkel, Schulman, Bullock, Moore, & Segundo, 1964; Hoppensteadt, 1986; see Figure 5). In another possible model, the RCO has intrinsically generated subthreshold oscillations that become suprathreshold with an appropriate DC input. The frequency of such oscillations is often controlled by the input (Llinas, Grace, & Yarom, 1991). Both subthreshold and suprathreshold intrinsic oscillations often present close-to-linear input-output (current to frequency) transfer functions (Calvin, 1975; Llinas et al., 1991; Silva, Amitai, & Connors, 1991). This implies that the input-rate to output-frequency transfer function of these oscillators is close to linear, since the amount of input current accumulated during a cycle is directly related to the rate of synaptic activation.

Three different frequencies are associated with an RCO. The *intrinsic frequency* ($f_c = 1/T_c$) is the RCO's frequency when the input to the RCO is quiescent. The *local frequency* is the RCO's frequency when the input to the PLL is quiescent, a situation that may include spontaneous activity within the loop. The *working frequency* ($f_o = 1/T_o$) is the RCO's average frequency during the decoding of a specific input.

2.3 Simulation. Validation of the basic idea of a neuronal PLL circuit and a demonstration of such a circuit's operation is provided by a simulation of a simple circuit that includes only the essential elements of the iPLL (see

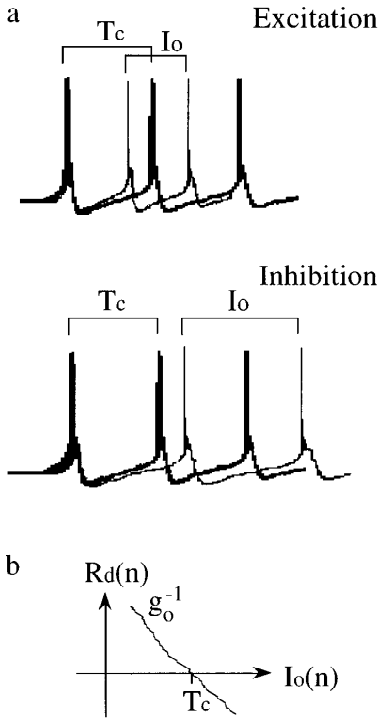

Figure 5: A neuronal RCO mechanism. (a) Output signal. The thick traces describe the membrane voltage of an RCO with no modulating input—when the RCO oscillates at its intrinsic frequency. Additional excitation or less inhibition will increase the depolarization slope, and thus increase the frequency of the RCO's output (top, thin trace). Additional inhibition or less excitation will decrease the slope, and hence decrease the frequency (bottom, thin trace). (b) A schematic transfer function of the RCO plotted as in Figure 2b. As the input (R_d) increases, the ISI (I_o) decreases.

Figure 6a). The simulation was performed on a DEC 3100 workstation using Genesis, a general-purpose neuronal simulator (Wilson & Bower, 1989). Neurons were represented by two compartments: one that represented an excitable soma that obeyed Hodgkin-Huxley kinetics and another that represented the dendrites. Three types of synapses were simulated: (1) *fast-excitatory*, non-NMDA-like synapses with a conductance time constant (τ) of 1 ms; (2) *slow-excitatory*, NMDA-like synapses with $\tau = 20$ ms, and (3) *slow-inhibitory*, $GABA_B$-like synapses with $\tau = 20$ ms. Axons were simulated as delay lines that conducted action potentials. Intrinsic oscillations were simulated by increasing the maximal sodium conductance by approximately

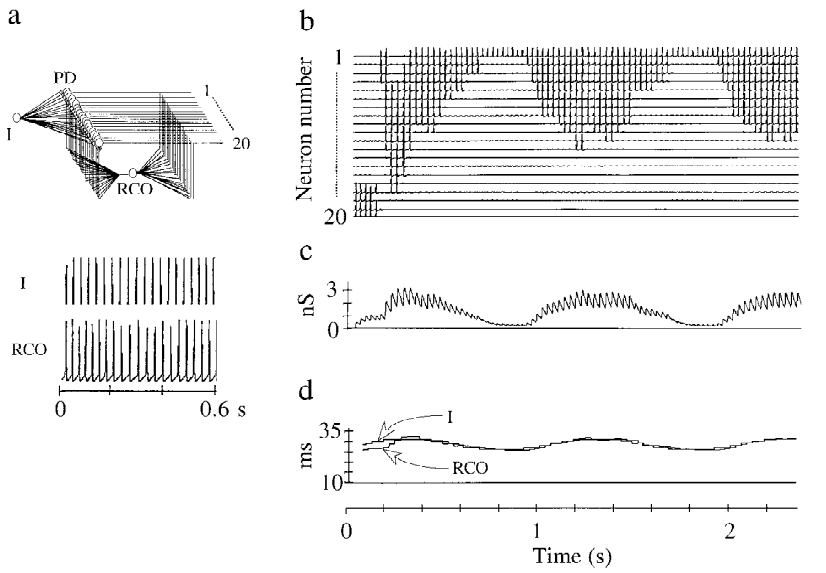

Figure 6: Computer simulation of a neuronal PLL circuit. (a) Simulated circuit and spike trains. The circuit was composed of one input cell (I), 20 PD neurons (PD), 20 different delay lines from the input to the PD neurons, and one RCO neuron (RCO) receiving an inhibitory input from each of the 20 PD neurons. The timings of the input spikes and the membrane voltage of the RCO are presented at the bottom. (b) The PLL's output, which is the population output of the PD. The spike trains of the 20 PD neurons are depicted. Each line represents, as a function of time, the membrane voltage of one PD neuron. (c) The RCO's integrated input—the total inhibitory conductance caused by synaptic input to the RCO neuron. (d) The instantaneous ISIs of the input I and the RCO are described as a function of time. After a lock-in stage, the two curves essentially merge.

50% (Alonso & Llinas, 1989; Llinas et al., 1991; Silva et al., 1991). The intrinsic oscillating frequency of the simulation was set by tuning the membrane capacitance.

The width of the loop was set to $w = 20$. The input was simulated by a single input cell (I) whose output was conveyed to the PD neurons via 20 axons, whose delays to the 20 PD neurons were uniformly distributed between 14 and 20 ms and which formed fast-excitatory synapses on PD neurons. All 20 PD neurons converged on a single RCO neuron via slow-inhibitory synapses. For simplicity, the INH neurons were discarded and replaced by direct inhibitory connections from the PD to the RCO. A single RCO neuron represented the hypothesized 20 RCO neurons. This RCO neuron fed back, by slow-excitatory synapses, each of the PD neurons.

The ability of this simplistic simulated PLL circuit to decode periodic modulations of periodic input signals was tested by "injecting" excitatory intracellular currents into the input cell's soma. Figures 6b–d depict the results of one simulation. The input signal was a 1 Hz modulation of a carrier frequency (35 Hz), with a modulation depth of 20%. The RCO frequency locks to the input frequency (see Figure 6d); the instantaneous ISI, of both the input and the RCO, are described by the two curves. After a lock-in stage, the two curves merge, which indicates the frequency locking. In the locked condition, the input modulation of 1 Hz is decoded by the PLL and approximated by a 1 Hz population signal (both population vector and population sum) at the PD's output (see Figure 6b). At any given time, both the population vector (the actual firing neurons) and the population sum (total spikes across the population) represent the input ISI (within the PD resolution limits). The integrated inhibition (see Figure 6c) modulates the RCO's frequency. This integrated signal is an integration of the PLL's output, and it provides a measure of the population sum.

This simple simulated circuit was able to decode modulations of up to 2 Hz with a 20% modulation depth. However, one cannot learn about the decoding limitations of the PLL from this simulation, since only a specific, limited circuit was simulated. For example, the resolution of PLL decoding depends on the number of elements, and the range of decodable modulation depths and frequencies, as well as lock-in dynamics, depends on the loop gain. This simulation mainly demonstrates how PLL neuronal signals should look in principle. To demonstrate the dependency of lock-in dynamics on the loop gain, I performed a MATLAB simulation of the iPLL, using equations A.4, A.9, and A.15 (see Figure 2) and a periodic PD function with the profile depicted in Figure 4d. The results are shown in Figure 7. All time variables are expressed in T_c (the RCO's intrinsic period; see appendix A.2) units. For an input period (T_i) of 1.2 T_c and an initial phase difference $[\eta_o(0) - \eta_i(0)]$ of 0.3 T_c, lock-in time was one cycle for loop gain $(G) = -1$ (see Figure 7a). When G was too small in absolute value (lowermost trace) the RCO could not approach the input period. The reason was that with such gains, the phase difference that was required to follow T_i exceeded the PD's working range ($T_c/2$; see Figure 4d). Thus, with this specific PD function, the working range of the iPLL was $T_c < T_i \leq T_c(1 + |G|/2)$. iPLLs with $G < -2$ (upper-most oscillating trace) were not stable (see appendix A.2, equation A.17). Between these two limits of G, iPLLs could lock in to the input, where lock-in times increased with increased deviation of G from -1. However, lock-in times also depended on the initial phase difference (see Figure 7b). Thus, even with ideal PLLs, having $G = -1$, lock-in to the onset of an input train might take more than one cycle, due to the phase difference. A single cycle lock-in is guaranteed only when the PLL is already locked to the input and a sudden change in the input periodicity is introduced, as demonstrated in Figure 7c. Here, after four cycles of

1.1 T_c the input ISI was changed to 1.4 T_c and from then on was modulated around 1.25 T_c with a modulation period of 10 T_i and a modulation depth of 0.4 (peak-to-peak). Six iPLLs with $0.5 \leq G \leq 1.75$ were simulated. Lock-in to the input onset was not immediate, due to the nonoptimal initial phase difference (0.3 T_c). However, after the PLLs were locked, those who could track the maximal input period (those with $G \leq -1$, see working ranges above) tracked it more or less smoothly. The tracking errors are plotted in Figure 7d. It can be seen that the iPLL with $G = -1$ (x's) tracked the input modulations with no errors, while the other iPLLs exhibit tracking errors, as expected (see section 2.1 and appendix A.3). The output rate produced by the iPLL with $G = -1$ is depicted in Figure 7e. Finally, the PLLs that could reach the maximal T_i (those with $G \leq -1$ in this case) were able to follow the highest possible rate of input modulations: ($2T_i$) (see Figure 7f).

Note that the maximal rate of input modulations trackable by PLLs does not indicate the maximal resolution of temporal decoding by PLLs. The latter is determined by the smallest deviation of input ISI that can be detected by a PLL and is determined by the resolution of the PD's population output (e.g., the resolution of the y-axis in Figure 7e). Thus, PLLs can detect (and represent by rate) temporal changes with a resolution that can be much higher than the maximal rate of temporal modulations that they can track. For example, a PLL whose working range is 100 ms $< T_i \leq$ 150 ms can, with enough PD resolution, distinguish between inputs of 110 ms and 111 ms, although it cannot track 1 kHz modulation.

3 Tactile PLLs

The mammalian tactile system contains the neuronal elements required for the function of thalamocortical PLLs. Following is a proposal for a plausible implementation of PLLs by the primate tactile system. The peripheral tactile system, which acquires sensations during exploration of textures, has been described in detail over the past three decades. The tactile system includes the three following subsystems, which are classified according to the temporal nature of their responses: slowly adapting (SA) receptors and neurons, which respond optimally over the low range (∼0–20 Hz) of stimulus frequencies; rapidly adapting (RA) receptors and neurons, which respond best over frequencies of medium range (∼20–40 Hz); and Pacinian (PC) receptors and neurons, which mainly transfer information at high frequencies (>80 Hz) (Talbot et al., 1968; Freeman & Johnson, 1982; Johansson, Landstrom, & Lundstrom, 1982; Goodwin, John, Sathian, & Darian-Smith, 1989). The glabrous fingertip is innervated mainly by RA receptors, by lower numbers of SA receptors, and by only a small number of PC receptors (Johansson & Vallbo, 1979; Darian-Smith & Kenins, 1980).

Less is known about the central mechanisms underlying tactile decoding and processing. The tactile pathways from the periphery to the cortex preserve the phase of the stimulus (Darian-Smith & Oke, 1980; Mountcas-

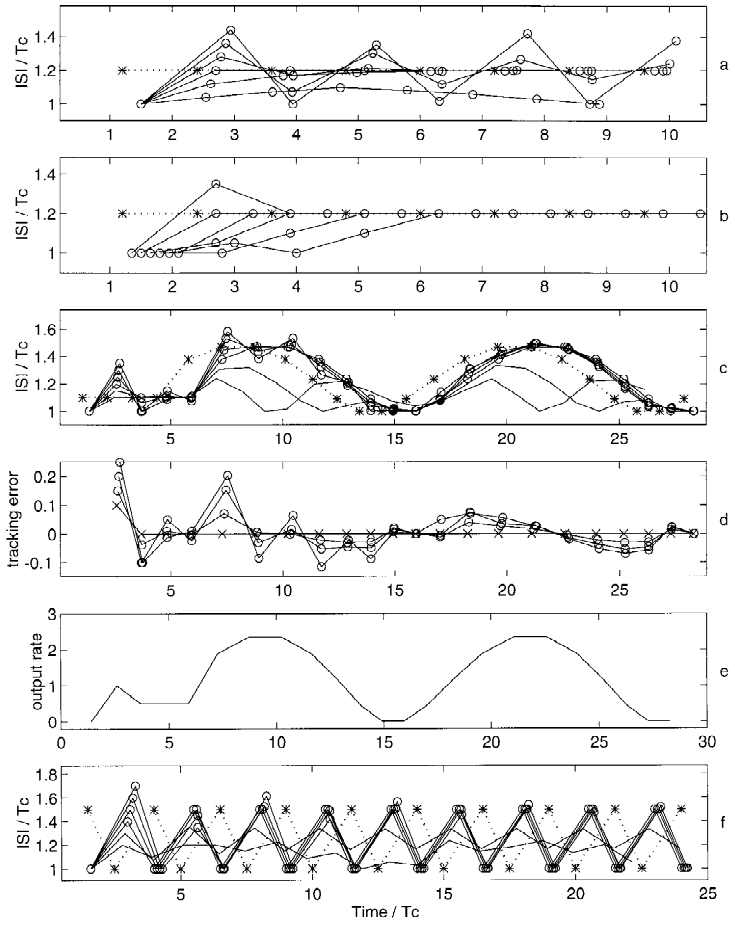

Figure 7: Dependence of lock-in dynamics on input parameters. The iPLL algorithm was simulated in MATLAB (see text). Simulations steps (n) were counted from 1. (a) Input (stars and dotted line): A steady input period at $T_i = 1.2T_c$. G values (traces from bottom up at $n = 2$): 0.2, 0.6, 1.0, 1.4, 1.8, 2.2. Initial phase difference $[\Delta\eta(1)] = 0.3T_c$ (b) Input: As in a. $G = -1$. $\Delta\eta(1) = 0.15, 0.30, 0.45, 0.60, 0.75, 0.90\ T_c$. (c) Input: Four cycles of $1.1T_c$ followed by $I_i(n) = (1.25 + 0.25\sin(2\pi(n-4)/10))T_c$, for $n > 4$. G values (traces from bottom up at $n = 2$): 0.5, 0.75, 1.0, 1.25, 1.5, 1.75. iPLLs with $G > -1$ are plotted without symbols. $\Delta\eta(1) = 0.3T_c$. (d) Tracking errors for the simulation in c were computed as $(I_o(n) - I_i(n-1))/T_c$, for $n > 1$. Only $G \leq -1$ are shown. $G = -1$ is plotted with X's. (e) The PLL's output rate (R_d), in arbitrary units, for the simulation in c. (f) Input: $T_i = 1.25\ T_c$, modulation rate ($2T_i$), modulation depth 40%. G values as in c. $\Delta\eta(1) = 0.1T_c$

tle, Talbot, Sakata, & Hyvärinen, 1969; Ferrington & Rowe, 1980; Burton & Sinclair, 1991; Gardner, Palmer, Hamalainen, & Warren, 1992). However, the degree of phase locking gradually decreases along the afferent pathways, with the largest reduction probably occurring at the transition from the thalamus to the cortex, a transition that is also accompanied by an increased complexity of response (Darian-Smith, Sugitani, Heywood, Karita, & Goodwin, 1982; Sinclair & Burton, 1988; Burton & Sinclair, 1994). This increased complexity could be due to significant processing that occurs already at the thalamocortical level (Gottschaldt, Vahle-Hinz, & Hicks, 1983).

3.1 Temporal Encoding of Textures. I consider here only textures (of variable patterns and heights) on flat surfaces (e.g., textures of sandpapers, clothes, woods, artificial gratings, or braille pages). A finger traversing these types of surfaces usually moves along sections of approximately straight lines (see Figure 8, top). The information contained in these textures consisting of a collection of ridges is expressed by three variables: amplitude, average spatial period (where period is 1 / frequency), and local spatial modulations. The information carried by the average spatial period (X_i) is called here the *roughness* of the surface and the information carried by local spatial modulations (p_i) the *pattern* of the surface. I use *italics* to distinguish this specific stimulus-defined *roughness* from the more general roughness percept. As I will show below, decoding *roughness* information can contribute to the roughness percept.

When a surface is transversed by fingertips, the spatial information is encoded in two ways:

1. Spatial encoding: Across the contact area ($\sim$0.6 cm^2 in humans), at any given moment, the spatial features are reflected by the corresponding skin deformations leading to a spatially encoded response of the relevant receptor population.
2. Temporal encoding: At any given skin location, receptors are responding to the fluctuations of the indentation amplitude produced by the movement (see section A.6).

Spatial encoding is probably best mediated by the SA receptors (Phillips, Johansson, & Johnson, 1990) and needs to be decoded by mechanisms utilizing spatial comparisons. Temporal encoding is probably best mediated by RA (and, to a lesser degree, PC) receptors, which respond reliably to temporal modulations (Darian-Smith & Oke, 1980; Morley & Goodwin, 1987). Such temporally encoded signals could be efficiently decoded by thalamocortical PLLs. However, since point skin indentations are modulated by both amplitude (due to vertical surface fluctuations) and time (due to horizontal interval fluctuations; see Figure 8, top), the interpretation of the decoded signals could be ambiguous. Electronic implementations of PLL, facing similar problems, always include an amplitude limiter at the input

stage (Gardner, 1979). Interestingly, the RA peripheral system employs a similar mechanism. Responses of RA mechanoreceptive fibers to vibratory stimuli, or moving spatial gratings, having amplitudes between fewer than 10 to hundreds of microns, are often of a 1:1 type; they fire one and only one spike per vibratory or grating cycle, regardless of the amplitude (Talbot et al., 1968; Darian-Smith & Oke, 1980; Goodwin & Morley, 1987; Gardner & Palmer, 1989). Every RA fiber exhibits a 1:1 response within a specific range of amplitudes (termed the "plateau" range; Talbot et al., 1968) and temporal frequencies (Darian-Smith & Oke, 1980). Outside these ranges, fibers respond with bursts of variable lengths per cycle (Darian-Smith & Oke, 1980; Morley & Goodwin, 1987), depending on the force and frequency of the stimulus (Darian-Smith & Oke, 1980; Goodwin et al., 1989).

Thus, in the case of the RA system and with a constant finger velocity, the encoding of the horizontal features of textures is straightforward. The horizontal (or temporal) modulations of the periodic indentation profile, as a function of x (or t), can be described by the two methods used above to describe temporal periodic signals (see Figure 1 and appendix A.1): either with respect to an imaginary "carrier" signal (see Figure 8a, $P_i(n)$) or with respect to the spatial intervals themselves (see Figure 8a, $p_i(n)$) (see appendix A.6). During scanning, the timing of the nth mechanoreceptive spike is uniquely determined by the location of the nth ridge (see Figure 8b). If the response type is 1:1, the RA mechanoreceptive fibers should fire one and only one spike per every ridge in the surface, and the sensory transformation takes a simple form: the horizontal spatial structure is directly represented by the temporal structure of the RA spike trains (see appendix A.6). With different ranges of finger forces, the 1:1 response becomes a 1:n response, and the transformation is more complex. However, as long as the duration of the bursts is small relative to the input average cycle (which is usually the case; Darian-Smith & Oke, 1980; Morley & Goodwin, 1987), decoding efficiency should hardly be affected since input onset times, which are the important parameters for the decoding, are not affected. Yet the increased input intensity and duration caused by the bursts should be compensated by a proper tuning of the PLL's loop parameters (S. Serulnik & E. Ahissar, unpublished observations). Thus, for optimal performance, PLL parameters should be tuned according to the expected form of input bursts.

3.2 Decoding by Thalamocortical PLLs. As I will show, the decoding of tactile signals by PLLs requires an additional feedback loop. Thus, the postulated temporal tactile decoder, as one module within a global tactile texture decoder, includes many parallel PLLs embedded within a sensorimotor feedback loop (see Figure 9). According to the model, the movement of fingers across a surface activates skin mechanoreceptors (MR) which convert the spatial details into temporal signals. The RA and PC mechanoreceptors at the fingertip include amplitude limiters (L), which eliminate amplitude modulations. The parallel array of input filters (IF; mechanoreceptors and

their fibers) transfers the filtered signal to an array of somatotopic organized PLLs, each specifically tuned to a particular frequency restricted to one of the tactile submodalities (SA, RA, or PC). Therefore, every point on the skin is driving a set of PLLs, each tuned to a particular frequency (see Dykes,

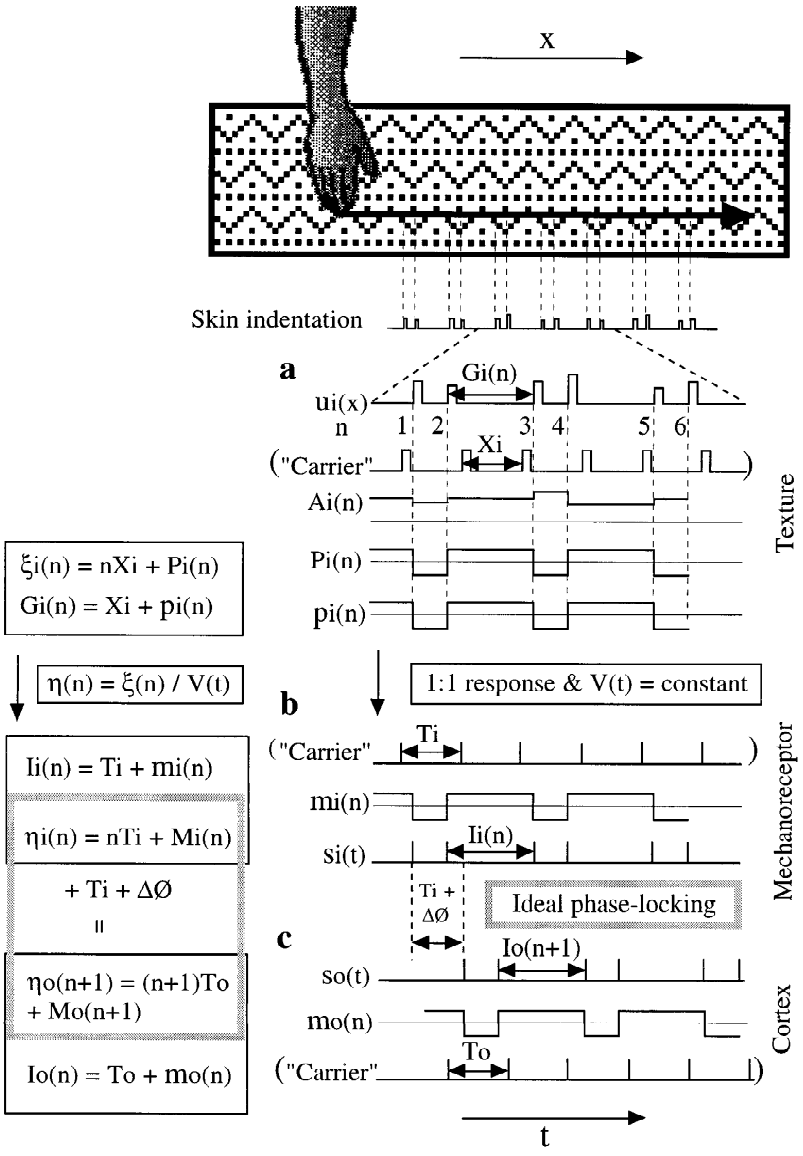

1983). The output of all the PLLs is fed to two readout networks, IP and IR, for *pattern* and *roughness* evaluation, respectively. The IR's output drives the velocity controller (VC), which closes the loop by controlling the finger velocity.

Each PLL thus processes information about different spatial frequencies of the explored surface. How does the brain know which PLLs provide relevant information about the actual surface being explored and how can it focus on these PLLs? If the PDs employ nonperiodic, sigmoid-like transfer functions, the answer to the first question would be simple. Only PLLs that are tuned to the relevant (i.e., informative) temporal frequencies should present modulated output signals. All other PLLs should produce outputs that are saturated at either the highest or the lowest possible values. Thus, the modulation depth of the AC output component, or a related measure such as $|R_{ac}(t)|$, should provide a reliable measure of the amount of information contained in each PLL's output. This criterion appears to be valid also for periodic PDs (like the one in Figure 4d). As the input average frequency moves away from the center of the working range, the probability of the instantaneous frequencies to exceed the bounds of this range increases. Once the input frequency exceeds one of these bounds, the PLL's output is closer to its average value, and its modulation depth decreases. Thus, local maxima of $|R_{ac}(t)|$ represent maximal information. Furthermore, it is most likely that these local maxima will be graded among different PLLs, and a global maximum will also be available. The reason is that each PLL can obtain a larger

Figure 8: *Facing page*. Illustration of a temporal encoding of spatial features. The movement of the hand (arrow) across a surface generates skin displacements at the zone of contact. This series of displacements can be described as a spatial signal $[u_i(x)]$ that represents the texture in this one-dimensional direction of movement. (a) Decomposition of the spatial signal. $u_i(x)$ can be decomposed into vertical $[A_i(n)]$ and horizontal [either an imaginary "carrier" $+P_i(n)$, or $p_i(n)$] components. The similarity between $P_i(n)$ and $p_i(n)$ in this example is due to the regularity of the *pattern*. $G_i(n)$ is the interridge interval. (b) Receptor transformation. Assuming a 1:1 response of mechanoreceptive fibers and a constant velocity, $u_i(x)$ is converted to a temporal signal described by $s_i(t)$. The temporal signal, which is carried by the mechanoreceptive fibers, can be also decomposed into subcomponents. However, due to the 1:1 response, which neglects amplitude changes, the amplitude component is constant and equal to 1, and thus is ignored. $I_i(n)$ is the ISI. Refer to appendix A.1 for the definitions of other terms. (c) Decoding by an ideal PLL. The phase-locking mechanism of the PLL forces the RCO's output $[s_o(t)]$ to track the peripheral input $[s_i(t)]$ with a delay of one cycle (T_i) and a constant phase difference $(\Delta\varnothing)$. As a result, the brain can extract the modulation ($M_o(n)$ or $m_o(n)$) that describes the *pattern* and the average interval (T_o) that describes the *roughness*. See appendices A.1, A.3, and A.6 for explanation of other symbols.

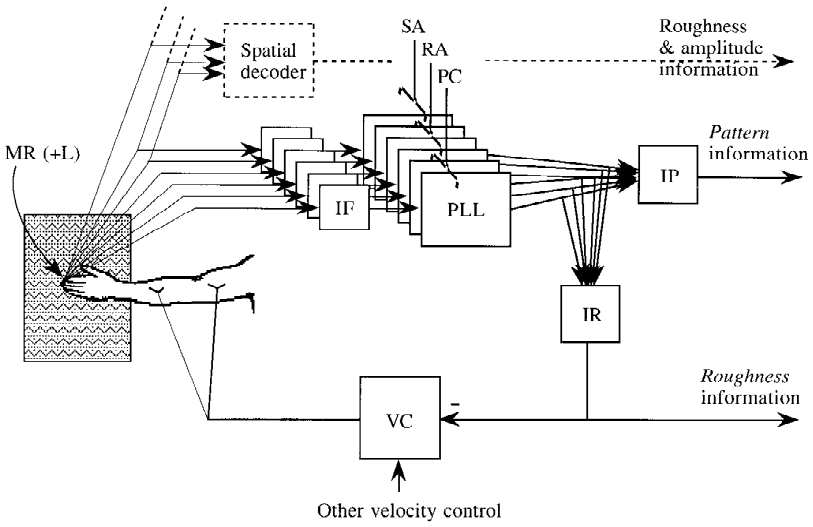

Figure 9: PLLs within a global texture decoder. Many topographically-organized PLLs reside in parallel; only six are shown in the figure. Each PLL is tuned to a specific frequency range within a specific submodality: SA, RA, or PC. The input of each PLL is received from a set of mechanoreceptive fibers through a set of dorsal column nuclei relay neurons, which together comprise the input filter (IF). Most of the mechanoreceptors (MR) include amplitude limiters (L). IP and IR are readout networks that produce *pattern*- and *roughness*-related information, respectively. A hypothetical spatial decoder illustrates the operation of additional mechanisms in parallel.

working range if it tunes the slope of its PD function according to its average frequency—smaller slopes for lower frequencies. In this case, the global maximum will indicate the PLL whose working range is fully exploited.

Since neuronal excitation is often sensitive to the variability at the input (Aertsen, Erb, & Palm, 1994), circuits that detect maximal variabilities can be implemented. If such circuits are included in the PLLs' readout networks (e.g., IP in Figure 9), they can assist the selection of one of the submodalities (SA, RA, or PC) and the specific PLLs within that submodality that are most informative. Other factors affecting this selection probably include visual, cognitive, and additional tactile information, such as that obtained by spatial decoders (see Figure 9). According to this selection, the finger velocity is deliberately determined to be in the range that will generate temporal frequencies in the appropriate range for the chosen PLLs. By setting the finger velocity, the system focuses on the selected PLLs, since they will generate the most informative output. To keep this focus steady, an automatic feed-

back system is required to carry out the fine-tuning of the velocity. Such a feedback system could be tuned to maximize the amount of output information from the selected set of PLLs, using $|R_{ac}(t)|$ as a measure. Although such an operation makes sense, I propose that if it is implemented, it is implemented as a higher-order feedback loop. For maintaining the input frequencies around a selected PLLs' working point, such a feedback system could simply operate on fluctuations of the averaged PLL's output, R_{dc}.

Let us represent each selected group of PLLs by a single PLL. Once a particular PLL is selected, the sensorimotor circuit responsible for temporal decoding can be described by two loops (see Figure 10a): the inner loop is the selected PLL, which extracts the input temporally encoded information (see Figure 8) and recodes it by rate (see appendix A.7), and the outer loop is an automatic velocity control (AVC), which keeps the input frequency of the PLL centered around the PLL's working frequency. IP and IR are reduced in this description to single filters, assumed to produce outputs related mainly to the selected PLL. The other inputs to IP and IR are assumed to be averaged out. The general case of processing, in which the average input frequency can change (albeit slowly) over time, even beyond the working range of the PLL, is assumed here. Thus, both the average input ISI and the average PLL's output are functions of time ($T_i(t)$ and $R_{dc}(t)$, respectively).

3.2.1 The automatic velocity control (AVC). When the PLL is locked, the average RCO's ISI is approximately equal to the average input ISI ($T_o(t) \approx T_i(t)$; see appendix A.3). If either the average input spatial period ($X_i(t)$) or the finger velocity ($V(t)$) is changed, the PLL will move to a new working point in which $T_o(t) \approx T_i(t)$. Such a new working point will be associated with a new average output rate ($R_{dc}(t)$) of the PLL. However, if the working range of the PLL is limited, as is the case for any practical implementation, this adaptive process is also limited, and consistent drifts in the input average frequency can eventually lead to a loss of locking as the PLL leaves its working range. From the point of view of the sensorimotor system, there are two possible solutions to this problem: it can either have many PLL circuits, each tuned to a different working range (the open-loop approach), or it can actively maintain the input temporal frequency within a working window (the closed-loop approach). The closed-loop approach, whose operation is postulated here, requires that, while operating near the center of the PLL's working range, if $T_o(t)$ is driven toward the limits of the working range, an action will be taken to bring $T_i(t)$ back to its original value via the control of the finger velocity, $V(t)$ (see appendix A.8).

The algorithm for the tactile AVC is composed of five elements (see Figure 10a): (1) a multiplier (MR), which multiplies the finger velocity by the spatial frequency of the texture; (2) a PLL circuit, which converts the *roughness* and *pattern* information to the DC and AC components of a rate signal; (3) a base-band filter (BBF), which transfers only the frequencies related to the *pattern*; (4) a low-pass filter (LPF), which transfers only the frequencies

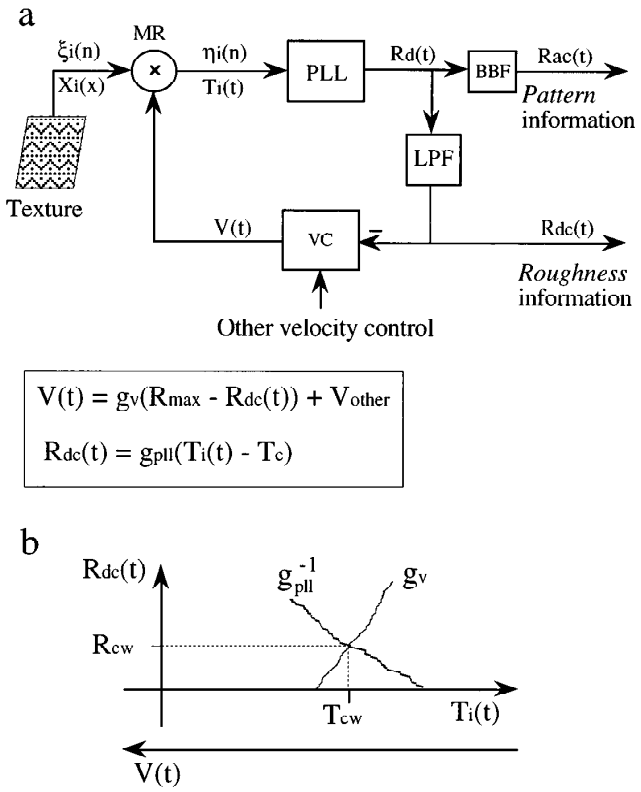

Figure 10: The algorithm of the AVC loop. (a) Loop components. MR, multiplier that includes an amplitude limiter; PLL, one of the PLL circuits in Figure 9 that is selected for optimization; BBF, base-band filter; LPF, low-pass filter; VC, velocity controller. $\xi i(n)$, location of the nth input ridge; $X_i(x)$, average interridge interval; $\eta_i(n)$, timing of the nth input spike; $T_i(t)$, average input ISI; $R_d(t)$, firing rate of the PLL's output; $R_{ac}(t)$, the integrated signal representing the *pattern*; $R_{dc}(t)$, the integrated signal representing changes in *roughness*; $V(t)$, the finger velocity. The loop equations (inset) are explained in appendix A.8. (b) Schematic examples of transfer functions. The crossing point (T_{cw}, R_{cw}) is the working point of the AVC, which, optimally, fits the desired working point of the selected PLL.

related to changes in the *roughness*; and (5) a velocity controller (VC), which controls the finger velocity.

The negative feedback nature of the AVC maintains the PLL's mean input ISI close to the PLL's desired working point (T_{cw}, R_{cw}), which is the center of the working range of the selected PLL. An increase in either the average spatial frequency or the finger velocity will result in the input's average ISI decreasing, $R_{dc}(t)$ increasing, and $V(t)$ decreasing (see Figure 10 and sec-

tion A.8). As a result, $T_i(t)$ will be driven back toward T_{cw} with a dynamics that depends on the actual l transfer functions. An opposite reaction occurs when either the average spatial frequency or the finger velocity decreases. Note that this servo operation holds for any given transfer functions, provided that they establish a negative feedback. Thus, dependence of tactile inputs on motor outputs (Chapman, 1994; Nelson, 1996) should affect the details of the AVC operation but not its principles.

3.3 Implementations of Tactile PLLs.

3.3.1 Implementations of tactile PDs. The tactile RA system appears to have evolved such that thalamic RA "relay" cells can be used as efficient phase detectors. The main features of the RA system contributing to this efficiency are (1) a rectangular-like distribution of the conduction velocities of RA fibers (Talbot et al., 1968; Darian-Smith & Kenins, 1980); (2) a close-to-uniform receptor sensitivity across the receptive field (Johansson & Vallbo, 1983; Gardner & Palmer, 1989); and (3) slow (long duration) cortical-to-relay neurons excitatory postsynaptic potentials (EPSPs) (Deschenes, Paradis, Roy, & Steriade, 1984). In general, the first two of these features are also typical of the PC, but not of the SA, subsystem; the third is probably common to all three of the tactile subsystems.

If organized correctly, the lemniscal input to the thalamic relay neurons can implement a square-wave-like signal, like in Figure 4c. Given features 1 and 2 of the RA system, the lemniscal input contains subpopulations in which, for a given point stimulus, different subsets of the input are active at different times. A "point" stimulus—an abrupt indentation at a single skin locatio—will generate a uniform response across all RA receptors that include that point in their receptive field, due to the uniform sensitivity of each receptor across its receptive field. When light touch is used, the skin indentation is assumed to be within a plateau range of amplitudes where the response has the form of one spike per one point stimulus (Talbot et al., 1968; Darian-Smith & Oke, 1980). If each subpopulation of fibers that share a skin location contains fibers with different conduction velocities, these activations will arrive at the thalamic relay neurons at different times for each fiber, like in Figure 4b. In this case, each of the fibers can be considered as a delay line generating a specific delay from skin activation to the firing of a lemniscal fiber. For the conductance velocities (Talbot et al., 1968; Darian-Smith & Kenins, 1980) and hand length ($\sim$50 cm) of monkeys, the spread of lemniscal firings probably contains mainly latencies between 7 and 14 ms, not including the duration of input bursts. This range corresponds to about one-fourth of a cycle of 30 Hz oscillations and is a reasonable range for a PD (see section 2.2.1). However, different spreads of the afferent signal are optimal for different PLL working frequencies. Thus, it is expected that channels conveying lower frequencies will employ larger temporal spreads.

3.3.2 Implementations of tactile RCOs. Obvious candidates for RCOs are the posterior SII local oscillators (Ahissar & Vaadia, 1990). Many of the neurons in this area display oscillatory patterns; however, not all of them can be considered local oscillators. At least 15% of the neurons in that area probably oscillate due to local mechanisms (Ahissar & Vaadia, 1990). The rest of the oscillating neurons (about 30% of the population) are either externally driven by the local oscillators, or their local oscillations are masked by a significant amount of noncorrelated input. The local oscillators can either directly drive thalamocortical neurons, if they project to the thalamus, or drive corticothalamic neurons. Note that these single-cell oscillations do not merely reflect sleeplike thalamocortical spindles (Steriade, McCormick, & Sejnowski, 1993) since they appear in wakefulness, include mainly gamma frequencies, and are not correlated among neighboring neurons.

There is no direct evidence yet that indicates an RCO-like operation of the SII oscillating neurons. However, these neurons lose their oscillatory patterns when stimulated with nonperiodic tactile stimuli (Ahissar & Vaadia, 1990). This finding is consistent with the cortical oscillators trying to track the nonperiodic input. More important, the distribution of oscillating frequencies of these oscillators matches the peripheral distribution of best frequencies (see Figure 11). A more direct evidence was obtained for SI oscillators in monkeys, employing RA frequencies (∼30 Hz; Lebedev & Nelson, 1995), and in rodents, employing whisking frequencies (∼10 Hz; Ahissar, Alkon, Zacksenhouse, & Haidarliu, 1996). These oscillators can be entrained by tactile periodic stimuli near their spontaneous frequencies, but usually not with significantly higher or lower frequencies. Thus, PLL circuits might exist in parallel in thalamocortical loops involving SI and SII cortices.

3.3.3 Implementation of Readout Networks. Each of the two readout networks, IP and IR, should implement at least two functions. The simple one, which is required for the AVC operation, is filtering out the unnecessary information. Both low-pass and bandpass filters are easy to implement by neuronal networks, utilizing synaptic integrations and decays. In addition, these networks should probably include circuits that compute and compare input variabilities (IP) and input averages (IR). Detailed implementations of these filters are beyond the scope of this article. Although the PLLs' outputs are described as converging to the readout networks (see Figure 9), they do not necessarily have to converge. The readout networks can utilize parallel processing and produce population outputs. Accordingly, the single lines standing for the outputs of the two filters in Figure 9 denote the unity of information conveyed by their outputs rather than the outputs' physical widths.

4 Discussion

4.1 Advantages and Limitations of PLLs. The PLL algorithm is used extensively in electrical engineering for decoding of phase and frequency

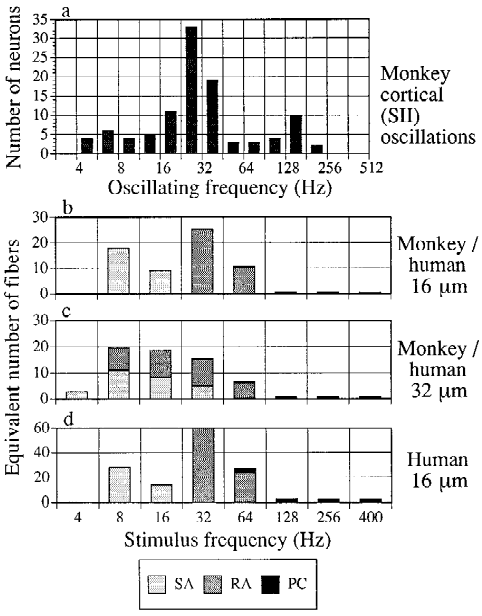

Figure 11: Cortical oscillating frequencies and peripheral frequency tunings. (a) Distribution of oscillating frequencies of cortical (posterior SII) single-cell oscillators (104 frequencies observed in 76 neurons of which 18 exhibited more than a single frequency). Only frequencies larger than 2.8 Hz were included for compatibility with the peripheral data. (modified from Ahissar and Vaadia, 1990). (b–d) Estimated distributions of peripheral tuning to the frequency of sinusoidal skin displacements. Ordinates depict estimations, for each input frequency, of the number of mechanoreceptive fibers that innervate the skin contact area and are tuned to that frequency. The distribution of tuning to vibratory frequencies among the input fibers was estimated here by calculating the "equivalent number of fibers" tuned to each frequency. The equivalent number of fibers per submodality is the fraction of the average response of that submodality at each frequency multiplied by the average number of fibers of the same submodality that innervates the stimulated area of skin. During light touch, the contact areas of skin for humans and monkeys are $\sim$0.6 cm^2 (Lamb, 1983) and $\sim$0.2 cm^2 (Goodwin & Morley, 1987), respectively. (b) Mean responses of mechanoreceptive fibers were obtained from data published for humans (Johansson et al., 1982) and innervation densities from data published for monkeys (Darian-Smith & Kenins, 1980). Skin contact area was assumed to be 0.2 cm^2. Peak-to-peak indentation amplitude is 16 μm. (c) Same as b, except that the indentation amplitude is 32 μm. (d) Same as b, except that the innervation densities were obtained from data published for humans (Johansson & Vallbo, 1979) and skin contact area was assumed to be 0.6 cm^2.

modulated signals, frequency synthesis, and pulse synchronization. When utilized as a phase demodulator, a PLL exhibits an excellent noise immunity due to its adaptive narrowband filtering (Gardner, 1979). This narrowband filtering is achieved by comparing the input against a specific internal frequency and becomes adaptive because of the feedback control of the internal frequency.

In principle, temporally encoded neuronal signals (see Figure 1) are phase-modulated signals; therefore, utilization by the brain of a PLL mechanism to decode temporally-encoded signals should be advantageous. However, there are limitations inherent in the PLL mechanism that the brain would have to compensate for. One limitation arises from the adaptive behavior of the PLL, which limits the PLL's capacity to track rapid changes in the input. As with any other negative feedback loop, a few input cycles may be needed before the PLL can lock in to a new input and efficient decoding can commence. Nevertheless, learning-induced fine tunings of the loop parameters can reduce to a minimum (down to 1 cycle) the number of lock-in cycles.

Another limitation of PLLs stems from the limited working ranges of their implementations. A PLL cannot track, although it can detect input modulations that are larger than its working range. The working ranges of basic neuronal PLLs are usually around half a cycle, with the upper limit probably being one cycle (see section 2.2). Thus, a typical, "nonsophisticated," neuronal PLL is limited to inputs with modulation depths of less than 50%. If an RCO cannot produce the required frequencies, the PLL's working range will be even more limited. This limitation can be circumvented by having several PLL circuits in parallel, each tuned to a different frequency range and decoding a different segment of the input information. In addition, "sophisticated" implementations of PDs can extend working ranges and reduce lock-in times.

A significant advantage of neuronal PDs is that transitions from one implementation to another can occur within a given anatomical circuit by changing cellular parameters. For example, at low excitability levels, a PD neuron can implement an AND-like function, at high excitability levels an OR-like function, and at intermediate excitability levels an AOR-like function (see section 2.2.1.3). Thus, neuronal PLLs can dynamically change their loop parameters, including gain and working range, to accommodate to global sensory changes or requirements. For example, a full-cycle working range can be implemented by asymmetrical PDs that employ an AND-like function for negative phase differences [$\eta_o(n) - \eta_i(n) < 0$] and an OR-like function for positive phase differences. In such an asymmetrical AOR-like PD, the order of input activation determines the sensitivity of the PD neurons. The periodic PD transfer function of such asymmetrical PDs has the shape of a sawtooth instead of the triangular shape of the symmetrical PDs (see Figure 4d). The advantages of a sawtooth PD function are that the

working ranges are larger, and with very large input modulations, the PLL immediately shifts to another valid working range.

Other options that are probably available for neuronal PLLs are dynamic tuning of the RCO's local frequency, asymmetric RCO transfer functions, and combined excitatory-inhibitory implementations of PLLs (see Figure 3a) with asymmetric or dynamically shifted relative weights.

4.2 Plausible Sites for PLLs. Neuronal circuits that contain local oscillators probably can function as PLLs without any specific tuning. In principle, the feedback connections and the basic phase detection function of any neuron (see section 2.2.1.1) establish the essential requirements of the loop. Nevertheless, efficient operation at a specific frequency range requires additional tuning of the cellular and circuit parameters (see section 2.2). Some neuronal systems have at least some of the required parameters for efficient PLLs. Following is a summary of the requirements from the circuitry and local oscillators and a review of plausible sites.

4.2.1 Potential Circuits. The sensory thalamocortical loops are attractive candidates for PLL circuits, since PLL performance improves when the RCO-to-PD connections are massive, and having PLLs early in a processing stream would be advantageous for facilitating sensory-sensory integration. Nevertheless, feedback circuits within or between cortical areas could function as PLLs as well. Within thalamocortical loops, the natural implementation would be that the thalamic relay neurons function as PDs and corticothalamic neurons at deep cortical layers function as RCOs. Natural candidates for INH neurons in iPLLs are the cortical inhibitory interneurons in layer 4 (White & Keller, 1987; Agmon & Connors, 1992; Swadlow, 1995). However, other combinations, including inhibitory neurons of the reticular nucleus of the thalamus, or oscillatory neurons in superficial layers that drive the corticothalamic neurons, are also possible, as long as the loop transfer functions establish a stable negative feedback loop (see appendix A.2). Within thalamocortical systems, many PLLs are expected to function in parallel, each tuned to a different combination of receptive field and working range.

4.2.2 Local oscillators. In a PLL, a local oscillator should function as an RCO, that is, its output frequency should be controllable by the input. The RCO's oscillations can be sub- or suprathreshold during spontaneous activity, as long as when decoding starts, the oscillations become suprathreshold. With single or groups of cells, which are oscillating due to intrinsic mechanisms, control of the frequency of oscillations by the input is expected to obey the simple neuronal rules required by the PLL: excitatory inputs should increase the frequency of oscillations, whereas inhibitory inputs should decrease the frequency (see section 2.2.2). Thus, single-cell oscillators are excellent candidates for RCOs. In contrast, oscillations generated outside the

processing network are not expected to be affected by the excitation levels of the network and thus cannot function as RCOs. The effect of neuronal input on a network that oscillates due to specific connectivity of excitatory and inhibitory cells is not obvious and depends on the exact connectivity and the exact input. Thus, neuronal ensembles that exhibit network oscillations will not be considered candidates for RCOs but rather as circuits that can be driven by RCOs.

Brain activity contains oscillations in a wide range of frequencies, from circadian to millisecond ranges. However, only frequency ranges compatible with perceptual time scales, during which sensory temporal codes should be transferred to motor rate codes, will be discussed here. Emphasis will be placed on the 10–100 Hz range, although lower and higher frequencies can probably also be used for perceptual processing by PLLs.

4.2.3 The primate somatosensory system. Candidates for somatosensory RCOs were presented in section 3.3.2. If PLLs indeed operate in somatosensory thalamocortical circuits, network oscillations that occur in the primary somatosensory and motor areas (reviewed in Fetz, 1993) during the performance of tactile tasks or during periods with global excitation could be due to propagation of the working frequencies from the PD neurons to the sensorimotor areas. If input modulations are not overly strong, the working frequency is preserved in the synchronous PD firings, even though the firing rate of the whole population might be modulated (see Figure 6).

4.2.4 The rodent vibrissal system. Many rodents achieve tactile sensory acquisition with an active process in which their whiskers move back and forth in a sinusoidal-like manner with frequencies near 10 Hz (Welker, 1964; Simons, 1995). Rodents use such whisking to localize (Welker, 1964) and identify objects with strategies and resolution capabilities comparable to those of primates achieved by applying manual active touch (Simons, 1995). During active whisking, the vibrissal pathway of the rat oscillates synchronously at around 10 Hz (Nicolelis, Baccala, Lin, & Chapin, 1995). These oscillations probably originate in the cortex, but in every cycle, the peripheral neurons fire first, followed by the firing of cortical ones, which in turn is followed by a firing of thalamic neurons. These observations are fully consistent with PLL circuits of 10 Hz operating in the thalamocortical vibrissal system of the rat. Recently we observed that cortical oscillators in the somatosensory cortices of anesthetized rats and guinea pigs exhibit three modalities of oscillating frequencies, at roughly 1, 10, and 100 Hz (Ahissar et al., 1996). It is possible that the ~10 Hz oscillators are utilized in PLLs that detect the location of external objects and that the ~100 Hz oscillators are utilized in PLLs that decode the texture of these objects (see Carvell & Simons, 1995).

4.2.5 The auditory system. Under normal conditions, most of the single-cell oscillations in the auditory cortex have frequencies below 14 Hz (Ahissar & Vaadia, 1990). Thus, if auditory PLLs exist, they probably decode low-frequency information derived from relatively slow processes such as speech or movements of sound sources (Ahissar, Ahissar, Bergman, & Vaadia, 1992).

4.2.6 The olfactory system. Network oscillations occurring in the olfactory system (Freeman, 1975) are probably utilized to enhance cortical processing or to encode sensory information (Hopfield, 1995), but not to decode temporally encoded sensory information which is not conjectured in this sense.

4.2.7 The visual system. During stimulations, the visual pathway often exhibits synchronous, wide-band oscillations (Neuenschwander & Singer, 1996; Engel et al., 1992; Eckhorn, 1994). Whether these oscillations are utilized for the decoding of temporally encoded information or for recoding spatially encoded information is not yet clear. The fact that the internal frequencies are usually much higher than the so-called temporal frequencies of the stimulus (i.e., the frequencies at which single receptors are stimulated) is not indicative in this case. The temporal structure of the retinal output depends also on the frequency of the sequential activation of neighboring receptors since, at least in cats, several receptors usually converge onto single ganglion cells. The direct dependency of cortical frequencies on stimulus velocities (Gray, Engel, Konig, & Singer, 1990; Eckhorn, Frien, Bauer, Woelbern, & Kehr, 1993) supports the direct coupling between peripheral and cortical oscillations. Visual temporal decoding by PLLs could rely on single-cell oscillators in the thalamus or the cortex. Neurons in the lateral geniculate nucleus (LGN) exhibit spontaneous stable oscillations (Ghose & Freeman, 1992) that are disturbed once visual patterns are presented, which is consistent with these oscillators trying to track modulated temporal structures. Neurons in superficial layers of the cortex exhibit intrinsic oscillations during stimulations (Gray & McCormick, 1996). These neurons could function as RCOs probably only after initial sensory or internal preparatory excitation.

4.2.8 Summary. The perceptual mechanisms of two sensory (tactile and visual) systems that apparently can use PLL circuits involve motion of the sense organs during sensory acquisition. Such movements result in encoding of spatial information in temporal firing patterns, information that can be efficiently decoded by PLL circuits. Hand movements can easily be measured with a resolution higher than that of the tactile receptive fields, while such measurements with eye movements are difficult (Carpenter, 1988). Thus, accurate testing of PLL's predictions in visual systems is limited. PLLs might be implemented differently in these two systems. For example, tactile RCOs are expected to be cortical, whereas visual ones could be thalamic.

According to the PLL model, the network oscillations observed in the visual and sensorimotor cortices reflect oscillatory activities in either the output or the readout stages of PLL circuits.

After the cessation of oscillatory sensory stimulations in both the visual and somatosensory modalities, the brain persists in emitting synchronized oscillations having the same frequency of the stimulus (Narici et al., 1987). This "oscillatory memory" requires a closed-loop operation, at either the cellular or the circuit level, as suggested by the PLL model. Testing of this phenomenon at low frequencies revealed that best resonating frequencies for the somatosensory modality were 6 and 8 Hz and for the visual modality 10 Hz. It will be interesting to see whether similar phenomena occur with oscillations around 30 Hz in the somatosensory system and 40 to 100 Hz in the visual system.

4.3 Experimental Evidence for Thalamocortical Tactile PLLs. Current physiological and anatomical data are compatible with PLL's being implemented within and across the thalamic ventrobasal nuclei (VB), SI, and SII areas. Neurons that can be considered as local oscillators in the SA, PC, and mostly RA ranges exist in SI and SII areas of primates (see section 3.3.2). The high percentage of posterior SII oscillators and the grouping of oscillators with frequencies that correspond to the three submodalities (see Figure 11) suggests an important role for SII in temporal decoding of textures. In fact, lesions in SII of primates significantly impair tactile texture decoding (Murray & Mishkin, 1984; Carlson, 1990). Furthermore, the direct motor connections of SII to the primary motor cortex (MI) (Jones, 1986; Burton, 1986) would facilitate participation of SII in a basic sensorimotor loop, such as the one described by the AVC loop.

The input tactile channels are evidently not fully segregated; sensory information is probably shared by different frequency channels and even between different submodalities. Thus, the decoding details cannot be as simple as described here. However, if channel segregation holds to a certain degree, PLL-like decoding could occur, and in this case the decoding principles outlined in this article should hold. Note that although anatomical continuity within input channels is required for input pathways running up to the cortex and back to the thalamus, physiological consistency of response type is required only up to the thalamus. In fact, the PLL model suggests that a significant code transformation occurs at the thalamocortical level. Thus, the findings that cortical response types are not correlated with peripheral ones (e.g., Tremblay, Ageranioti-Belanger, & Chapman, 1996) are not in conflict with the PLL model.

Below are presented data that are consistent with (i.e., can be explained by) the PLL model and data that support the model (i.e., that are more consistent with the PLL model than with other models). Since no other specific mechanism has yet been suggested for texture decoding at the circuit

level, the PLL will be compared with the open-loop model of local oscillators (Ahissar, 1995) and with "non-PLL" mechanisms in general.

4.3.1 Data consistent with PLLs functioning in the tactile thalamocortical system.

- The RA system employs amplitude limiting, uniform receptive fields, and temporal dispersions, all required for efficient thalamic phase detection (see sections 3.1 and 3.3.1).
- The RA pathway exhibits a high degree of phase locking that preserves the temporal information up to the thalamus (see the introduction to section 3).
- The mechanoreceptors and their fibers act as bandpass filters; they emphasize a certain range of the input frequency spectrum (Johansson et al., 1982; Freeman & Johnson, 1982; Goodwin et al., 1989), as required for efficient PLL decoding.
- The reciprocal connections between the thalamus and cortex are modality and somatic specific (Jones, 1986; Doetsch, Standage, Johnston, & Lin, 1988; Hoogland, Welker, & Van der Loos, 1987).
- The circuitry required for the function of thalamocortical ePLLs and iPLLs exists in mammals (Jones, 1986; White & Keller, 1987; Agmon & Connors, 1992).
- Thalamic relay neurons are activated with short EPSPs from afferent projections and long EPSPs from cortical inputs (Deschenes et al., 1984), an arrangement that facilitates thalamic PD operation (see section 3.3.1).
- Oscillating frequencies of SI neurons can be controlled locally (Silva et al., 1991; Amitai, 1994; Ahissar et al., 1996).
- Two successive stimuli to the same location on the skin are not differentiable for delays between 0 and 15–40 ms (Rosner, 1961), consistent with a PLL-like mechanism that "samples" the input using RA-range frequencies.
- Talbot et al. (1968) suggested the existence of a central mechanism that "alters its own activity [which "measures"] the dominant period in the input train of impulses." The PLL, by altering its own activity (the RCO's frequency), can "measure" the dominant input period.

4.3.2 Data that support PLLs in the tactile thalamocortical system.

- Local oscillators in SI of monkeys (Lebedev & Nelson, 1995) and of anesthetized rats and guinea pigs (Ahissar et al., 1996) can be entrained by oscillatory tactile stimuli when the input frequency is close to the local frequency.

- When vibratory stimuli are applied within series of decreasing intensities, minimal detection thresholds were consistently slightly lower than during series of increasing intensities (Talbot et al., 1968). Whereas this result cannot be explained by neural mechanisms involving adaptation or habituation, it is easily explained by PLL-like mechanisms: A minimal input intensity is required to lock in the PLL (increasing series), but once the PLL is locked (decreasing series), less input intensity is necessary to keep it locked, since the local oscillators already fire in phase with the input.
- A qualitative coding transformation, from temporally oriented at the thalamus (Sinclair, Sathian, & Burton, 1991) to rate oriented at the cortex (Sinclair & Burton, 1991), appears to occur at the thalamocortical level of monkeys performing a texture discrimination task. The gradual nature of the cortical responses is more consistent with the PLL than with alternative open-loop mechanisms producing labeled-line coding (Ahissar, 1995).

4.3.3 Data consistent with inhibitory PLLs.

- There is evidence "that presumed inhibitory interneurons in the cat SI could be activated first by thalamic inputs among cortical neurons and set to inhibit the output cells" (Yamamoto, Samejima, & Oka, 1988, p. 199).
- Activities of local oscillators in SI of the behaving monkey are often inhibited by vibrotactile stimuli (Lebedev & Nelson, 1995).
- Local oscillators in SI of the rat receive strong inhibitory input (Chagnac-Amitai & Connors, 1989).
- With SII neurons of cats, firing in phase with a vibratory stimulus is impaired when GABA receptors are blocked (Alloway, Sinclair, & Burton, 1988). This is consistent with cortical phase locking being achieved by inhibitory PLL circuits.
- In response to thalamic (VB) stimulation, corticothalamic neurons in SI of cats exhibit inhibitory postsynaptic potentials (Landry & Dykes, 1985). Synaptic excitation is also observed in some of these neurons, which suggests a combination of ePLLs and iPLLs.
- Somatosensory cortical neurons of rats have been classified according to whether they are coactivated with fast ($\sim$20 Hz) electroencephalogram waves (CoE cells) or not (CoI cells) (Angel, 1983). CoE neurons exhibit rhythmic firing around 20 Hz, dominate the electroencephalogram when CoI neurons are quiet, respond to peripheral inputs with longer latencies then CoI neurons, and activate thalamic (reticular) cells with a shorter latency then CoI neurons do. All of these

phenomena are consistent with CoE functioning as RCO neurons and with CoI functioning as inhibitory interneurons (INH).

- About 25% of the SI neurons of the monkey exhibit a sharp, positive sigmoidal dependency on the spatial period (Sinclair & Burton, 1991; see also Darian-Smith et al., 1982), as expected by iPLLs (see Figure 6). Negative sigmoidal dependency, as predicted by ePLLs, was not observed.

4.3.4 Data that seem inconsistent with PLLs in tactile thalamocortical systems.

- Although the primary function of the proposed PLLs in tactile thalamocortical systems would be in perception of patterns, these PLLs should, using only temporal input information, be able to convey information about the roughness of the scanned texture. However, in some cases, estimation of roughness is independent of the temporal parameters of the peripheral input (Lederman, 1981). This would imply that even if PLL circuits exist in the somatosensory system, their contribution to the perception of roughness is negligible. However, so far, only a partial range of possible conditions has been studied—for example, only spatial frequencies of relatively high frequencies (groove widths of 0.175–1 mm; Lederman, 1981). Also, the involvement of temporal information was tested only after subjects were trained to estimate the roughness of different textures at different velocities. Since the nervous system is capable of developing perceptual constancies over many parameters, one of which is probably finger velocity, naive rather than trained subjects should have been used. When naive subjects are required to identify forms or discriminate gratings, perception indeed depends on finger velocity (Vega-Bermudez, Johnson, & Hsiao, 1991; Ahissar & Gamzu, 1995). Furthermore, during training with a difficult discrimination task, subjects developed scanning strategies that were based on maximizing differences between temporal frequencies by controlling the scanning hand velocities (Gamzu, Haidarliu, & Ahissar, 1994).

- As the spatial frequency of the stimulus decreases, the SA and RA mechanoreceptive fibers in the hand of the monkey fire more spikes per second, even if the peak temporal frequency of the stimulus is kept constant (Goodwin & Morley, 1987). This seems to contradict a basic assumption of the tactile PLL that peripheral firing depicts in a 1:1 manner the existence of texture ridges. These experiments were conducted with indentations (1 mm) well above the peripheral threshold (tens of microns; Talbot et al., 1968), which probably forced the peripheral fibers to function outside their plateau range (see Goodwin et al., 1989). Nevertheless, the spatial features were still represented by the peripheral temporal structure, though with a 1:*n* ratio (Mor-

ley & Goodwin, 1987; Goodwin et al., 1989). In principle, PLLs can decode 1:*n* input ratios, and the decoding efficiency depends on the parameters. For example, if the bursts increase the input spread (T_{wi}; see Figure 4) beyond $T_i/2$, performance could be impaired. However, if they bring T_{wi} closer to $T_i/2$, performance should improve. Since the length of these bursts increases as the spatial frequency decreases (Goodwin et al., 1989), they might indeed improve the efficiency of the putative PLLs. Note, however, that the peripheral burst lengths are not necessarily preserved at the outputs of the dorsal column nuclei.

- The PLL model for the tactile thalamocortical system predicts that the temporal information of the input will be represented by the firing rates of cortical populations. In contrast, Burton and Sinclair (1994) concluded that the cortex probably encodes spatial features of the surface independent of temporal factors. However, since only correlations between *average* values of cortical rates and hand velocities were computed, velocity was not systematically varied, and "velocity was not well controlled" (Sinclair & Burton, 1991, p. 165), these results cannot rule out representations of input temporal structures in cortical rates. Indeed, Chapmann and colleagues found recently, applying systematic variations of input velocities, that the firing rates of 66% of SI neurons are directly related to the stimulus velocity (Tremblay et al., 1996).

- Johnson and Lamb (1981) argued that the temporal dispersion caused by a wide distribution of conduction velocities of mechanoreceptive fibers, especially those of RA fibers, can contribute to a spatial dispersion (blurring) of the image of the scanned texture. This would indeed be the case with a central mechanism that blindly integrates input signals from all input fibers. However, a PLL-like mechanism can actually benefit from such dispersions, which convert input "click trains" to lemniscal square waves (see Figure 4c) and enable the PD operation (see sections 2.2.1 and 3.3.1).

- Connor and Johnson (1992) have compared spatial and temporal encoding schemes as possible candidates to underlie tactile roughness estimation and showed that spatial variations have the closest correlation with roughness estimations. However, in some spacing ranges, temporal variations are better than spatial variations in predicting the subjects' reports (compare Figures 9 and 10 in Connor & Johnson, 1992). A view consistent with this and other (e.g., Ahissar & Gamzu, 1995) studies is that different perceptual mechanisms are emphasized as a function of the task at hand and the range of the spatial frequencies being explored. Roughness estimation tasks and low-spatial-frequency pattern discrimination tasks are probably primarily dealt with by spatial mechanisms (Connor & Johnson, 1992, and Ahissar & Gamzu,

1995, respectively) while high-spatial-frequency pattern discrimination tasks are primarily dealt with by temporal mechanisms (Ahissar & Gamzu, 1995), such as the PLL. This is consistent with the finding that superimposed vibrations improve stationary grating resolution in a range of high spatial frequencies and decrease performance in a range of lower frequencies (Johnson & Phillips, 1981).

4.3.5 Summary of experimental evidence. Experimental data indicate that under certain conditions, operation of a PLL-like mechanism is feasible at the thalamocortical level of mammalian tactile systems. In this system, current data favor the existence of iPLLs over ePLLs, although combined operation of both implementations has been indicated. If such PLLs exist, they should function in parallel to other, nontemporal, decoding mechanisms.

4.4 Interactions with other tactile mechanisms. If PLL circuits do exist in the brain, it is likely that they do not exist as isolated circuits and they operate in parallel with other temporal and nontemporal decoding mechanisms. In fact, Johnson, Phillips, and colleagues have shown that some spatial features are most efficiently resolved by the SA system (Johnson & Lamb, 1981; Phillips & Johnson, 1981; Phillips et al., 1990), and this resolution appears to occur without significant dependency on temporal parameters (Phillips, Johnson, & Hsiao, 1988; Phillips, Johansson, & Johnson, 1992). They suggested that both "spatial" (involving the SA system) and "nonspatial" (involving the RA system) mechanisms underlie texture perception; the RA system probably encodes the microscopic dimensions and the SA the macroscopic dimensions of the texture (Johnson & Phillips, 1984). Similarly, I suggest that PLL circuits are embedded in and intermingled with other circuits and that, as a whole, these circuits function as a texture analyzer (Taylor, Lederman, & Gibson, 1973). Within such embedded and intermingled circuits, operations that obey PLL principles should occur in parallel to other operations that obey other principles. Other possible operations could be purely spatial, such as spatial variation detection (Connor & Johnson, 1992), or spatiotemporal, such as cross-coincidence detection among parallel phase-preserved input signals. In real time, the adaptive brain can emphasize one or another operation, according to the task at hand and previous experience. Thus, PLL circuits, which probably occur predominantly in the RA system, can decode temporal information related to the *pattern*—to the fine details of the surface—while spatial mechanisms (e.g., Bankman, Hsiao, & Johnson, 1990), which predominantly use the SA system, can decode rate-encoded information related to the macroscopic details (e.g., the roughness or shape) of textures. In addition, SA-based intensity mechanisms can refine *pattern* perception by using detailed spatial information, and PLL circuits can refine roughness perception by using fine temporal information.

4.5 Predictions of the Tactile PLL Model. The predictions derived directly from the algorithm are considered critical; a rejection of any one of them results in a rejection of the model or, at least, a major modification of it. A rejection of an implementation-specific prediction results in the rejection of only that specific implementation. The electrophysiological predictions require a distinction between two types of neurons: RCO neurons, which are local oscillators, and PD (or PD-driven) neurons, whose oscillating activity is externally driven. A partial list of both types of predictions follows. The implementation-specific predictions are detailed only for the AND-like, vector PDs (see section 2.2.1.2). For these implementations, the thalamocortical relay neurons can function as PDs only if the lemniscal input is subthreshold; therefore, the related predictions apply only for light touch, such as that used for texture discrimination.

Algorithm-Derived ("critical") Predictions.

AVC predictions.

a1. During a difficult identification of a patterned texture, the exploring velocities are expected to maintain the average temporal frequency of the input within one of the three ranges that correspond to the trimodal distribution of cortical oscillating frequencies (see Figure 11), with the RA range being preferred.

PLL predictions.

a2. RCO neurons are expected to track, within a range around their spontaneous oscillating frequency, variations in the frequency of a vibratory stimulus.

a3. When a periodic stimulus is applied at a frequency that matches the frequency of the RCO, the PD neurons are expected to be phase locked with both the stimulus and the RCO neurons, and, during phase-locking, the spikes of the PD neurons should usually (and in AND-like implementations always) lag those of the RCO neurons.

a4. When the loop is locked, the net excitatory input to the RCO should be a monotonic increasing function of the input frequency. This is because in order to follow a higher frequency, a neuronal RCO needs to be excited further.

a5. While the PLL is locked, as the frequency of the stimulus is increased, the delay between the input and the RCO neurons, $(\eta_0 - \eta_i)$, becomes more positive (see Figure 4d).

a6. Within the PLL's working range, the response of the PD population should be monotonic with the input frequency. The polarity of this relationship depends on the implementation (see Figure 3) and the measurement point (e.g., before or after an inhibitory stage).

Implementation-Specific ("Noncritical") Predictions for AND-Like Vector PDs.

Thalamocortical Implementations.

t1. Within groups (or "rods"; Jones, 1986) of thalamocortical relay neurons that share the same receptor modality, receptive field location, and cortical projecting area, different neurons will have different response latencies (phase shifts) that preferentially cover a range of several ms.

Excitatory PLLs (ePLLs).

e1. Usually an abrupt and strong peripheral stimulus should increase the instantaneous frequency of an RCO.

e2. The higher the input frequency, the higher the fraction of PD neurons that should respond to the input.

e3. Entrainment of single PD neurons should exhibit a steplike or sigmoidal dependency on input frequency. They should not be entrained to low frequencies and should start to respond once the input frequency becomes higher than a certain threshold.

e4. At low input frequencies, only PD neurons that respond with short latencies should respond. As the input frequency increases, additional PD neurons, which have incrementally longer response latencies, should be recruited. Thus, although all PD neurons can maintain phase locking at high-input frequencies, PD neurons with shorter response latencies should maintain phase locking to stimuli of lower frequencies.

Inhibitory PLLs (iPLLs).

i1. Usually an abrupt and strong peripheral stimulus should decrease the instantaneous frequency of an RCO.

i2. The higher the input frequency, the lower the fraction of PD neurons that should respond to the input.

i3. Entrainment of single PD neurons should exhibit a steplike or sigmoidal dependency on input frequency. They should be entrained to low frequencies and should stop responding once the input frequency becomes higher than a certain threshold.

i4. At high-input frequencies, only PD neurons that respond with long latencies should respond. As the input frequency decreases, additional PD neurons, which have decrementally shorter response latencies, should be recruited. Thus, although all PD neurons can maintain phase locking at low input frequencies, a PD neuron with a longer response latency should maintain phase locking to stimuli of higher frequencies.

Appendix

A.1 Temporally- and Rate-Encoded Neuronal Signals. Any spike train that consists of N spikes of a single neuron can be described as (see Figure 1a)

$$s(t) = \sum_{n=0}^{N-1} S(t - \eta(n)) \tag{A.1}$$

where $S(t')$ describes a single spike triggered at $t' = 0$ (see Figure 1a inset), and $\eta(n)$ describes the series of spike timings,

$$\eta(n) = \eta(0) + nT + M(n) = \eta(0) + nT + \sum_{j=1}^{n} m(j), \qquad n > 0 \tag{A.2}$$

where T is the average ISI; $M(n)$ is the "absolute" modulation of T for the nth spike and represents the deviation of the timing of the nth spike from the expected timing of the nth spike of the equivalent ideal oscillator having the same T; and $m(n)$ is the "cycle modulation" and represents the deviation of the nth ISI from T. By definition, the total modulation over the whole spike train should be zero

$$\left[M(N) = \sum_{j=1}^{n} m(j) = 0 \right].$$

For an ideal oscillator, $M(n) = m(n) = 0$ for every n. The instantaneous ISI is (see Figure 1a):

$$I(n) = \eta(n) - \eta(n-1) = T + m(n), \qquad n > 0 \tag{A.3}$$

$$\eta(n) = \eta(0) + \sum_{j=1}^{n} I(j), \qquad n > 0. \tag{A.4}$$

It is assumed, as a convention, that the spike train was not modulated prior to $n = 0$; therefore:

$$I(0) = T; \qquad m(o) = 0; \qquad m(j) = 0, \quad j < 0 \tag{A.5}$$

The information carried by the spike train is described by T and m. Generally the information carried by T and m could be referred to as rate-encoded and temporally-encoded, respectively, since T is a measure of the average firing rate over the whole period and m is a measure of the fine temporal modulations within that period.

A description of a signal by rate requires the division of a spike train into rate bins, with each rate bin being represented by a single number. Each of these single numbers can be evaluated by a variety of functions, ranging from a simple spike count to a weighted average that uses a postsynaptic filter function. Here, rate-encoded signals will be represented by simple spike counts over each rate bin. If other measurements are required, the spike count terms (e.g., $A(k)$ in equation A.6) should simply be replaced with other terms. Thus, a spike train can be described by a series of counts of spikes, where each count corresponds to a single rate bin (see Figure 1b):

$$R_x(t) = \sum_{k=0}^{Nr-1} A(k)R(t - kT_r), \tag{A.6}$$

where T_r is the rate bin, $R(t')$ is a pulse function that equals 1 for $0 \leq t' < T_r$ and 0 otherwise (see Figure 1b, inset), $A(k)$ is the spike count of the neuron at the kth rate bin, and N_r is the number of rate bins in the spike train.

For simplicity, negative "firing rates" will be ascribed to inhibitory inputs. Thus, a rate signal is defined as the difference between the count of spikes leading to EPSPs and the count of spikes leading IPSPs. For example, a single excitatory cell can produce only positive rate values, and a single inhibitory cell can produce only negative rate values.

Two kinds of population rate coding are considered here: population sum, which, per each rate bin k, is the sum of all $A_i(k)$, and population vector, which, per each rate bin k, is the array of all $A_i(k)$.

A.2 Phase-Locked Loop.

A.2.1 Rate-controlled oscillator. The RCO's output signal is:

$$s_o(t) = \sum_{n=0}^{N-1} S(t - \eta_o(n)) \tag{A.7}$$

where

$$\eta_o(n) = \eta_o(0) + nT_c + M_c(n). \tag{A.8}$$

T_c is the RCO's intrinsic period—its ISI when it receives no input—and $M_c(n)$ is the nth spike's absolute modulation (see equations A.2 and A.3 for other related definitions). The ISI (the "cycle") of the RCO is controlled by its input in the following way:

$$I_o(n) = T_c + g_o(R_d(n)), \tag{A.9}$$

where g_o, in the general case, is a monotonic decreasing or a monotonic increasing function, $g_o(0) = 0$, and $R_d(n)$ is the input to the RCO integrated over the interval preceding spike n, during $I_o(n)$ (see Figure 1 and

section 2.2.2). In neuronal implementations, g_o will probably always be a decreasing function in which the more positive (excitatory) the oscillator's input is, the sooner the oscillator will fire its next spike, and vice versa for more negative (inhibitory) inputs.

The average value of $R_d(n)$ is not necessarily, and usually will not be, 0. Therefore, T_c will not necessarily equal the average ISI of the RCO. To be consistent with equation A.3, for any given decoding period, $R_d(n)$ will be described as being composed of two components: a DC component (the average value, R_{dc}) and an AC component (the residual modulations, $R_{ac}(n)$):

$$R_d(n) = R_{dc} + R_{ac}(n), \tag{A.10}$$

and the average ISI of the RCO, T_o, will be:

$$T_o = T_c + \langle g_o(R_d(n)) \rangle, \tag{A.11}$$

where $\langle x \rangle$ is the average value of x over the described decoding period. Thus, the output timings of the RCO can be rewritten as:

$$\begin{aligned} \eta_o(n) &= \eta_o(0) + nT_o + M_o(n) \\ &= \eta_o(0) + nT_o + \sum_{j=1}^{n} m_o(j), \quad n > 0. \end{aligned} \tag{A.12}$$

For a linear g_o we get:

$$\langle g_o(R_d(n)) \rangle = g_o(R_{dc}), \tag{A.13}$$

and the instantaneous ISI is (from equations A.3, A.9, and A.11),

$$I_o(n) = T_o + g_o(R_{ac}(n)). \tag{A.14}$$

A.2.2 Phase detector. The PD's output, $R_d(n)$, is a rate-encoded signal, which is a function of the difference between the arrival times of the PD's two inputs,

$$R_d(n+1) = g_d(\eta_o(n) - \eta_i(n)), \tag{A.15}$$

where g_d is a monotonic increasing or a monotonic decreasing function. The difference $\eta_o(n) - \eta_i(n)$ is simply the difference between the times of appearance of the nth spikes of the RCO and the PLL's input, where n is counted only within a locked state, when the RCO's and the input's spikes are paired. With neuronal implementations, g_d probably cannot achieve a strict monotonic shape but rather will assume a staircase-like form. There will be ranges of phase difference within which the PD will produce a constant output. The size of these ranges determines the PD's resolution (see section 2.2.1) and, hence, also the PLL's resolution.

A.2.3 The loop gain. The ability of the PLL to be locked to the input depends on the loop's functioning as a negative feedback loop. In such a negative feedback loop, any deviation of the input from its expected frequency will produce an error signal (R_{ac}) that will drive the RCO's frequency in the direction that will reduce the error—in the same direction as the input's deviation. To provide a negative feedback, the gain along the loop during one cycle, referred to as the *loop gain*, should be negative. The loop gain, G, is computed per a *working point* (e.g., the crossing point in Figure 2b), assuming a constant input. It is equal to the gain of a small perturbation from the working point that is obtained after one cycle and is approximately (exactly for a linear system)

$$G \approx g'_o g'_d, \tag{A.16}$$

where, with continuous g_o and g_d, g'_o and g'_d are the derivatives of g_o and g_d, respectively, at the working point. With discrete g_o or g_d, g'_x equals $\Delta y/\Delta x$, where Δy is the output change generated by a minimal input change (Δx). The PLL will be stable only if any deviation from a working point, generated within the loop while the input is constant will be attenuated at the next cycle. A perturbation will be canceled at the next cycle if $G = -1$, will be attenuated if $-1 < G < 0$, and will be inverted and attenuated if $-2 < G < -1$. Outside this range, any perturbation will increase in absolute magnitude with each successive cycle. Thus, a necessary, although not sufficient, requirement for a stable PLL is

$$-2 < G < 0. \tag{A.17}$$

Therefore, to keep a PLL stable g_d and g_o must have opposite slopes around the working point (see, for example, Figure 2b). A range within which input modulations can be decoded is defined as a *working range* of the PLL. This range is determined by equation A.17, the dynamic range of the RCO, and the input average frequency.

A.3 Tracking. For clarity, let us consider an *ideal PLL*, in which the derivatives of g_d and g_o are constant (equal to k_d and k_o, respectively), $G = -1$, the RCO fires single spikes per cycle, and there is no noise. Suppose the input to the PLL (hereafter "the Input") is:

$$s_i(t) = \sum_{n=0}^{N-1} S(t - \eta_i(n)), \qquad I_i(n) = T_i + m_i(n), \qquad n > 0 \tag{A.18}$$

and

$$m_i(n) = 0, \qquad n \le 0.$$

When the loop is locked, there is one and only one RCO spike per each Input spike. If the Input is not modulated (i.e., it is perfectly periodic), the timings of the RCO's spikes will differ from the Input spikes only by a constant time delay (phase shift),

$$\eta_o(n) = \eta_i(n) + \Delta\varnothing \tag{A.19}$$

where $\Delta\varnothing$ is a constant time difference and n is the index of the Input cycle. And

$$I_o(n) = I_i(n). \tag{A.20}$$

When the Input is temporally modulated, the modulation is detected by the PD, which detects the difference between the expected $\eta_i(n)$ ("stored" as $\eta_o(n)$) and the actual timing. The detected difference corrects the RCO's frequency so that the latter matches the Input frequency. However, this correction will take place only at the following cycle $(n+1)$:

$$I_o(n) = I_i(n-1) \tag{A.21}$$

and, from equation A.3,

$$T_o + m_o(n) = T_i + m_i(n-1). \tag{A.22}$$

By definition, T_o is the average ISI of the RCO, and as long as the loop is locked, it is equal to the average Input ISI, T_i,

$$T_o = T_i \tag{A.23}$$

and, therefore,

$$m_o(n) = m_i(n-1). \tag{A.24}$$

Thus, the Input modulation is replicated by the RCO's modulation, with one cycle lag.

The average periods, T_o and T_i, are defined de facto for every decoding period. Thus, the PLL does not "know" the exact values for these averages during the decoding, and a decomposition of its output signal to the different components will fit the above definitions only at the end of the decoding period. Note, however, that this non-causal process relates only to the observer's interpretation of the decoding process and does not relate to the process itself, since the decoding utilizes the actual timings [$\eta_o(n)$ and $\eta_i(n)$] of the signals (equations A.9 and A.15).

A.4 Decoding. It can be shown that with ideal PLLs,

$$R_{dc} = g_d(\Delta\varnothing) \tag{A.25}$$

$$R_{ac}(n+1) = -g_d(m_i(n)) = g_o^{-1}(m_i(n)) \tag{A.26}$$

$$\Delta\varnothing = T_c - T_i + \varnothing_m. \tag{A.27}$$

$\Delta\varnothing$ is the average phase difference and, together with R_{dc}, determines the PLL's working point (see Figure 2b). $\varnothing_m$ is a constant delay that depends on the implementation (see section A.5.2).

If g_d or g_o is not linear, the AC component will depend on the DC component, that is, on the working point. However, since g_d (and g_o^{-1}) is monotonic, $R_d(n)$ is unique (within the resolution limits) for every input. When $G \neq -1$, the above solutions are the steady-state solutions that are obtained after a variable number of cycles, depending on G.

Using minimal rate bin ($= T_i$), the output of the ideal PLL is (see equation A.6),

$$R_d(t) = g_d(T_c - T_i + \varnothing_m) - \sum_{n=0}^{N-1}[g_d(m_i(n-1))R(t - nT_i)]. \tag{A.28}$$

Readout mechanism that employ longer rate-bins should sample or integrate the PLL's output.

A.5 PD Implementations.

A.5.1 A single neuron PD. The working range of such a PD is determined by the effective widths of its inputs—the maximal delay from an onset of an EPSP in which, if an EPSP from the other input is added, the membrane voltage will cross the threshold. For similar inputs whose (EPSP amplitude)/(threshold distance) $= A$

$$T_w = \tau \ln(A/(1-A)). \tag{A.29}$$

Assuming $\tau = 10$ ms is the decay time constant, if $A = 0.8$, the working range (T_w) is almost 14 ms, and if $A = 0.9$, it is about 22 ms.

A.5.2 Population PDs. Within the working range of the ePLL (T_{we}; see Figure 4d),

$$R_d(n+1) = R_{\max} + k_d[\eta_o(n) - \eta_i(n)], \qquad k_d > 0. \tag{A.30}$$

Since g_o is monotonic decreasing, $G < 0$ and the basic algorithm can be implemented straightforwardly by the circuit denoted by the dashed lines in Figure 3a. With the PD implementation of Figure 4d, the average delay is

$$\Delta\varnothing = T_c - T_i - R_{\max}/k_d. \tag{A.31}$$

Within the working range of the iPLL (T_{wi}, see Figure 4d),

$$R_d(n+1) = R_{\max} - k_d[\eta_o(n) - \eta_i(n)], \qquad k_d > 0. \tag{A.32}$$

In this case, $G < 0$ because of the INH that are added to the loop (see Figure 3a, solid lines). The average delay for the Figure 4d iPLL implementation is

$$\Delta\varnothing = T_c - T_i + R_{\max}/k_d. \tag{A.33}$$

The PLL's output, in both the excitatory and inhibitory implementations, is a population output.

A.6 Tactile Signals. It is assumed, for simplicity, that for any given scanning direction, all ridges have negligible widths. Textures consisting of a collection of such ridges can be described, along any one-dimensional direction, in a discrete form by

$$u_i(x) = \sum_{n=0}^{N} A_i(n)U[x - \xi_i(n)], \tag{A.34}$$

where $U(x')$ describes a single ridge at $x' = 0$ with a unit height, $A_i(n)$ is the height of the nth ridge, and $\xi_i(n)$ describes the location of the nth ridge,

$$\begin{aligned} \xi_i(n) &= \xi_i(0) + nX_i + P_i(n) = \xi_i(0) + nX_i + \sum_{j=0}^{n} p_i(j); \\ G_i(n) &= X_i + p_i(n), \end{aligned} \tag{A.35}$$

where X_i is the average spatial period, $P_i(n)$ is the absolute modulation of this period for the nth ridge, $p_i(n)$ is the cycle modulation, and $G_i(n)$ is the inter-ridge-interval (see section A.1). If a mechanoreceptor response is 1:1, then for a constant finger velocity, V, the sensory transformation is simply

$$\eta_i(n) = \xi_i(n)/V, \qquad \eta_i(0) = \xi_i(0) = 0, \tag{A.36}$$

and similar relationships hold for the signals' components:

$$T_i = X_i/V; \quad I_i(n) = G_i(n)/V; \quad m_i(n) = p_i(n)/V. \tag{A.37}$$

A.7 Tactile Decoding. With ideal PLLs, minimal rate bins ($= T_i$) and constant finger velocity, the two output components (see equations A.28 and A.37) are,

$$R_{dc}(t) = g_d(T_c - X_i(t)/V(t) + \varnothing_m) \tag{A.38}$$

$$R_{ac}(t) = -\sum_{n=0}^{N-1}[g_d(p_i(n-1)/V(t))R(t - nT_i)] \tag{A.39}$$

where $\varnothing_m$ is an implementation-specific delay.

A.8 Automatic Velocity Control. Suppose the desired working point is T_{cw}; then the requirement is that

$$X_i(t)/V(t) = T_{cw}, \qquad dx = V(t)dt, \tag{A.40}$$

and

$$V(t) = X_i(t)/T_{cw} \tag{A.41}$$

is the finger velocity that the AVC should produce. The AVC is a servo-regulating loop (see Figure 10) whose controlled variable, $T_i(t)$, should be kept constant. The loop equations are:

$$V(t) = g_v(R_{\max} - R_{dc}(t)) + V_{\text{other}} \tag{A.42}$$

$$R_{dc}(t) = g_{pll}(T_i(t) - T_c) \tag{A.43}$$

where g_{pll} and g_v are the PLL's and VC's transfer functions, respectively (see Figure 10b), $R_{\max}$ is the maximal possible $R_{dc}(t)$, V_{other} is the velocity additive component caused by the "other velocity control," and T_c is the PLL's intrinsic frequency (see appendix A.2).

Acknowledgments

I thank S. Serulnik and M. Zacksenhouse for extensive and illuminating discussions on phase-locked loops; A. Aertsen, M. Ahissar, D. Blake, T. Flash, K. O. Johnson, D. Shoham, A. Treves, S. Ullman, and several anonymous referees for their helpful comments on previous versions of this article; and B. Schick for reviewing the manuscript. This work was supported by the Alon Foundation, Israel; the Minna-James-Heineman Foundation, Germany; and grant 93-198 from the United States–Israel Binational Science Foundation, Jerusalem, Israel.

Note added in proof:
Recently we found that the behavior of cortical oscillators in the barrel cortices of anesthetized rats and guinea pigs confirms predictions a2 and a5. Also, the behavior of multi-units at the thalamic recipient layers of these cortices is consistent with predictions a5 (under the assumption of AND-like PD operation) and a6 (Ahissar, E., Haidarliu, S., & Zacksenhouse, M. (1997) "Decoding temporally encoded sensory input by cortical oscillations and thalamic phase comparators." *Proc. Natl. Acad. Sci. USA*. *94*:11633–11638). Note also that the results of Nicolelis et al. (1995) confirm prediction a3.

References

Abeles, M. (1982). Role of the cortical neuron: Integrator or coincidence detector? *Isr. J. Med. Sci*., *18*, 83–92.

Abeles, M., Bergman, H., Margalit, E., & Vaadia, E. (1993). Spatiotemporal firing patterns in the frontal cortex of behaving monkeys. *J. Neurophysiol*., *70*, 1629–1638.

Aertsen, A., Erb, M., & Palm, G. (1994). Dynamics of functional coupling in the cerebral cortex: An attempt at a model-based interpretation. *Physica-D*, *75*, 103–128.

Agmon, A., & Connors, B. W. (1992). Correlation between intrinsic firing patterns and thalamocortical synaptic responses of neurons in mouse barrel cortex. *J. Neurosci*., *12*, 319–329.

Ahissar, E. (1995). *Conversion from temporal-coding to rate-coding by neuronal phase-locked loops* (Tech. Rep. GC-EA / 95-4). Rehovot, Israel: Weizmann Institute of Science.

Ahissar, M., Ahissar, E., Bergman, H., & Vaadia, E. (1992). Encoding of sound source and movement: The activity of single neurons and interactions between adjacent neurons in the primary auditory cortex of monkeys. *J. Neurophysiol*., *67*, 203–215.

Ahissar, E., Alkon, G., Zacksenhouse, M., & Haidarliu, S. (1996). Cortical somatosensory oscillators and the decoding of vibrissal touch. *Soc. Neurosci. Abstr*., *22*, 18.

Ahissar, E., & Gamzu, E. (1995). Utilization of temporally-encoded versus spatially-encoded information during the performance of a tactile discrimination task. *Soc. Neurosci. Abstr*., *21*, 1018.

Ahissar, E., & Vaadia, E. (1990). Oscillatory activity of single units in a somatosensory cortex of an awake monkey and their possible role in texture analysis. *Proc. Natl. Acad. Sci. USA*, *87*, 8935–8939.

Alloway, K. D., Sinclair, R. J., & Burton, H. (1988). Responses of neurons in somatosensory cortical area II of cats to high-frequency vibratory stimuli during iontophoresis of a GABA antagonist and glutamate. *Somatosens. Mot. Res*. *6*(2), 109–140.

Alonso, A., & Llinas, R. R. (1989). Subthreshold Na^+-dependent theta-like rhythmicity in stellate cells of entorhinal cortex layer II. *Nature*, *342*, 175–177.

Amitai, Y. (1994). Membrane potential oscillations underlying firing patterns in

neocortical neurons. *Neuroscience, 63*, 151–161.

Angel, A. (1983). The functional interrelations between the somatosensory cortex and the thalamic reticular nucleus: Their role in the control of information transfer across the specific somatosensory thalamic relay nucleus. In G. Macchi, A. Rustioni, and R. Spreafico (Eds.), *Somatosensory integration in the thalamus* (pp. 222–239). Amsterdam: Elsevier.

Bankman, I. N., Hsiao, S. S., & Johnson, K. O. (1990). Neural image transformation in the somatosensory system of the monkey: Comparison of neurophysiological observations with responses in a neural network model. In *Cold Spring Harbor Symposia on Quantitative Biology* (Vol. 55, pp. 611–620). Cold Spring Harbor, NY: Cold Spring Harbor Laboratory Press.

Berkley, M. (1978). Vision: Geniculocortical system. In R. B. Masterton (Ed.), *Handbook of behavioral neurobiology, Vol 1: Sensory integration* (pp. 165–207). New York: Plenum Press.

Boussaoud, D., & Wise, S. P. (1993). Primate frontal cortex: Effects of stimulus and movement. *Exp. Brain Res., 95*, 28–40.

Buanomuno, D., & Merzenich, M. M. (1995). Temporal information transformation into a spatial code by a neural network with realistic properties. *Science, 267*, 1028–1030.

Burton, H. (1986). Second somatosensory cortex and related areas. In E. G. Jones and A. Peters (Eds.), *Cerebral cortex* (Vol. 5, pp. 31–98). New York: Plenum Press.

Burton, H., & Sinclair, R. J. (1991). Second somatosensory cortical area in Macaque monkeys: 2. Neuronal responses to punctate vibrotactile stimulation of glabrous skin on the hand. *Brain Res., 538*, 127–135.

Burton, H., & Sinclair, R. J. (1994). Representation of tactile roughness in thalamus and somatosensory cortex. *Can. J. Physiol. Pharmacol., 72*, 546–557.

Calvin, W. H. (1975). Generation of spike trains in CNS neurons. *Brain Res., 84*, 1–22.

Carlson, M. (1990). The role of somatic sensory cortex in tactile discrimination in primates. In E. G. Jones and A. Peters (Eds.), *Cerebral Cortex* (Vol. 8B, pp. 451–486). New York: Plenum Press.

Carpenter, R. H. S. (1988). *Movements of the eyes*. 2nd ed. London: Pion.

Carr, C. E. (1993). Processing of temporal information in the brain. *Annu. Rev. Neurosci., 16*, 223–243.

Carvell, G. E., & Simons, D. J. (1995). Task- and subject-related differences in sensorimotor behavior during active touch. *Somatosens. Mot. Res., 12*, 1–9.

Chagnac-Amitai, Y., & Connors, B. W. (1989). Synchronized excitation and inhibition driven by intrinsically bursting neurons in neocortex. *J. Neurophysiol., 62*, 1149–1162.

Chapman, C. E. (1994). Active versus passive touch: Factors influencing the transmission of somatosensory signals to primary somatosensory cortex. *Can. J. Physiol. Pharmacol., 72*, 558–570.

Connor, C. E., & Johnson, K. O. (1992). Neural coding of tactile texture: Comparison of spatial and temporal mechanisms for roughness perception. *J. Neurosci., 12*(9), 3414–3426.

Darian-Smith, I., & Kenins, P. (1980). Innervation density of mechanoreceptive fibres supplying glabrous skin of the monkey's index finger. *J. Physiol.*, *309*, 147–155.

Darian-Smith, I., & Oke, L. E. (1980). Peripheral neural representation of the spatial frequency of a grating moving at different velocities across the monkey's finger pad. *J. Physiol.*, *309*, 117–133.

Darian-Smith, I., Sugitani, M., Heywood, J., Karita, K., & Goodwin, A. (1982). Touching textured surfaces: Cells in somatosensory cortex respond both to finger movement and to surface features. *Science*, *218*, 906–909.

Deschenes, M., Paradis, M., Roy, J. P., & Steriade, M. (1984). Electrophysiology of neurons of lateral thalamic nuclei in cat: Resting properties and burst discharges. *J. Neurophysiol.*, *51*, 1196–1219.

Doetsch, G. S., Standage, G. P., Johnston, K. W., & Lin, C. S. (1988). Thalamic connections of two functional subdivisions of the somatosensory forepaw cerebral cortex of the raccoon. *J. Neurosci.*, *8*(6), 1873–1886.

Dykes, R. W. (1983). Parallel processing of somatosensory information: A theory. *Brain Res. Rev.*, *6*, 47–115.

Eckhorn, R. (1994). Oscillatory and non-oscillatory synchronizations in the visual cortex and their possible roles in associations of visual features. *Prog. Brain Res.*, *102*, 405–426.

Eckhorn, R., Frien, A., Bauer, R., Woelbern, T., & Kehr, H. (1993). High frequency (60–90 Hz) oscillations in primary visual cortex of awake monkey. *NeuroReport*, *4*, 243–246.

Engel, A. K., Konig, P., Kreiter, A. K., Schillen, T. B., & Singer, W. (1992). Temporal coding in the visual cortex: New vistas on integration in the nervous system. *Trends. Neurosci.*, *15*, 218–226.

Ferrington, D. G., & Rowe, M. (1980). Differential contributions to coding of cutaneous vibratory information by cortical somatosensory areas I and II. *J. Neurophysiol.*, *43*, 310–331.

Fetz, E. E. (1993). Cortical mechanisms controlling limb movement. *Curr. Opin. Neurobiol.*, *3*, 932–939.

Freeman, A. W., & Johnson, K. O. (1982). Cutaneous mechanoreceptors in Macaque monkey: Temporal discharge patterns evoked by vibration, and a receptor model. *J. Physiol.*, *323*, 21–41.

Freeman, W. J. (1975). *Mass action in the nervous system*. New York: Academic Press.

Gamzu, E., Haidarliu, S., & Ahissar, E. (1994). Sensorimotor control: Dependence of finger velocity on the scanned spatial frequency during performance and learning of a tactile task. *Isr. Soc. Neurosci.*, *3*, 57.

Gardner, F. M. (1979). *Phaselock techniques*. New York: Wiley.

Gardner, E. P., & Palmer, C. I. (1989). Simulation of motion on the skin. I. Receptive fields and temporal frequency coding by cutaneous mechanoreceptors of OPTACON pulses delivered to the hand. *J. Neurophysiol.*, *62*, 1410–1435.

Gardner, E. P., Palmer, C. I., Hamalainen, H. A., & Warren, S. (1992). Simulation of motion on the skin. V. Effect of stimulus temporal frequency on the representation of moving bar patterns in primary somatosensory cortex of monkeys. *J. Neurophysiol.*, *67*, 37–63.

Georgopoulos, A. P. (1986). On reaching. *Annu. Rev. Neurosci*., *9*, 147–170.
Ghose, G. M., & Freeman, R. D. (1992). Oscillatory discharge in the visual system: Does it have a functional role? *J. Neurophysiol*., *68*, 1558–1574.
Goldberg, J. M., & Brown, P. B. (1969). Response of binaural neurons of dog superior olivary complex to dichotic tonal stimuli: Some physiological mechanisms of sound localization. *J. Neurophysiol*., *32*, 613–636.
Goodwin, A. W., John, K. T., Sathian, K., & Darian-Smith, I. (1989). Spatial and temporal factors determining afferent fibre responses to a grating moving sinusoidally over the monkey's fingerpad. *J. Neurosci*., *9*(4), 1280–1293.
Goodwin, A. W., & Morley, J. W. (1987). Sinusoidal movement of a grating across the monkey's fingerpad: Effect of contact angle and force of the grating on afferent fiber responses. *J. Neurosci*., *7*(7), 2192–2202.
Gottschaldt, K.-M., Vahle-Hinz, C., & Hicks, T. P. (1983). Electrophysiological and micropharmacological studies on mechanisms of input-output transformation in single neurones of the somatosensory thalamus. In G. Macchi, A. Rustioni, & R. Spreafico (Eds.), *Somatosensory integration in the thalamus* (pp. 199–216). Amsterdam: Elsevier.
Gray, C. M., Engel, A. K., Konig, P., & Singer, W. (1990). Stimulus-dependent neuronal oscillations in cat visual cortex: Receptive field properties and feature dependence. *Eur. J. Neurosci*., *2*, 607–619.
Gray, C. M., & McCormick, D. A. (1996). Chattering cells: Superficial pyramidal neurons contributing to the generation of synchronous oscillations in the visual cortex. *Science*, *274*, 109–113.
Hoogland, P. V., Welker, E., & Van der Loos, H. (1987). Organization of the projections from barrel cortex to thalamus in mice studied with Phaseolus vulgaris-leucoagglutinin and HRP. *Exp. Brain Res*., *68*, 73–87.
Hopfield, J. J. (1995). Pattern recognition computation using action potential timing for stimulus representation. *Nature*, *376*, 33–36.
Hoppensteadt, F. C. (1986). *An introduction to the mathematics of neurons*. Cambridge: Cambridge University Press.
Jeffress, L. A. (1948). A place theory of sound localization. *J. Comp. Physiol. Psychol*., *41*, 35–39.
Johansson, R. S., Landstrom, U., & Lundstrom, R. (1982). Responses of mechanoreceptive afferent units in the glabrous skin of the human hand to sinusoidal skin displacements. *Brain Res*., *244*, 17–25.
Johansson, R. S., & Vallbo, A. B. (1979). Tactile sensibility in the human hand: Relative and absolute densities of four types of mechanoreceptive units in glabrous skin. *J. Physiol*., *286*, 283–300.
Johansson, R. S., & Vallbo, A. B. (1980). Spatial properties of the population of mechanoreceptive units in the glabrous skin of the human hand. *Brain Res*., *184*, 353–366.
Johansson, R. S., & Vallbo, A. B. (1983). Tactile sensory coding in the glabrous skin of the human hand. *Trends. Neurosci*., *6*, 27–32.
Johnson, K. O., & Lamb, G. D. (1981). Neural mechanisms of spatial tactile discrimination: Neural patterns evoked by braille-like dot patterns in the monkey. *J. Physiol*., *310*, 117–144.
Johnson, K. O., & Phillips, J. R. (1981). Tactile spatial resolution. I. Two-point

discrimination, gap detection, grating resolution, and letter recognition. *J. Neurophysiol.*, *46*, 1177–1191.

Johnson, K. O., & Phillips, J. R. (1984). Spatial and nonspatial neural mechanisms underlying tactile spatial discrimination. In C. von Euler, O. Franzen, V. Lindblom, and D. Ottoson (Eds.), *Somatosensory mechanisms* (pp. 237–248). London: Macmillan.

Jones, E. G. (1986). Connectivity of the primate sensory-motor cortex. In E. G. Jones & A. Peters (Eds.), *Cerebral cortex* (Vol. 5, pp. 113–184). New York: Plenum Press.

Lamb, G. D. (1983). Tactile discrimination of textured surfaces: Psychophysical performance measurements in humans. *J. Physiol.*, *338*, 551–565.

Landry, P., & Dykes, R. W. (1985). Identification of two populations of corticothalamic neurons in cat primary somatosensory cortex. *Exp. Brain Res.*, *60*, 289–298.

Lebedev, M. A., & Nelson, R. J. (1995). Rhythmically firing (20–50 Hz) neurons in monkey primary somatosensory cortex: Activity patterns during initiation of vibratory-cued hand movements. *J. Comp. Neurosci.*, *2*, 313–334.

Lederman, S. J. (1981). The perception of surface roughness by active and passive touch. *Bulletin of the Psychonomic Society*, *18*, 253–255.

Llinas, R. R., Grace, A. A., & Yarom, Y. (1991). *In vitro* neurons in mammalian cortical layer 4 exhibit intrinsic oscillatory activity in the 10- to 50-Hz frequency range. *Proc. Natl. Acad. Sci. USA*, *88*, 897–901.

Middlebrooks, J. C., & Green, D. M. (1991). Sound localization by human listeners. *Annu. Rev. Psychol.*, *42*, 135–159.

Morley, J. W., & Goodwin, A. W. (1987). Sinusoidal movement of a grating across the monkey's fingerpad: Temporal patterns of afferent fiber responses. *J. Neurosci.*, *7*, 2181–2191.

Mountcastle, V. B. (1993). Temporal-order determinants in a somatesthetic frequency discrimination—Sequential order coding. *Ann. N.Y. Acad. Sci.*, *682*, 150–170.

Mountcastle, V. B., Talbot, W. H., Sakata, H., & Hyvärinen, J. (1969). Cortical neuronal mechanisms in flutter-vibration studied in unanesthetized monkeys: Neuronal periodicity and frequency discrimination. *J. Neurophysiol.*, *38*, 452–484.

Murray, E. A., & Mishkin, M. (1984). Relative contributions of SII and area 5 to tactile discrimination in monkeys. *Behav. Brain Res.*, *11*, 67–83.

Narici, L., Romani, G. L., Salustri, C., Pizzella, V., Modena, I., & Papanicolaou, A. C. (1987). Neuromagnetic evidence of synchronized spontaneous activity in the brain following repetitive sensory stimulation. *Int. J. Neurosci.*, *32*, 831–836.

Nelson, R. J. (1996). Interactions between motor commands and somatic perception in sensorimotor cortex. *Curr. Opin. Neurobiol.*, *6*, 801–810.

Neuenschwander, S., & Singer, W. (1996). Long-range synchronization of oscillatory light responses in the cat retina and lateral geniculate nucleus. *Nature*, *379*, 728–732.

Nicolelis, M. A. L., Baccala, L. A., Lin, R. C. S., & Chapin, J. K. (1995). Sensori-

motor encoding by synchronous neural ensemble activity at multiple levels of the somatosensory system. *Science, 268*, 1353–1358.

Perkel, D. H., & Bullock, T. H. (1968). Neural coding. *Neurosci. Res. Prog. Bull., 6*, 221–248.

Perkel, D. H., Schulman, J. H., Bullock, T. H., Moore, G. P., & Segundo, J. P. (1964). Pacemaker neurons: Effects of regularly spaced synaptic input. *Science, 145*, 61–63.

Phillips, J. R., & Johnson, K. O. (1981). Tactile spatial resolution. II. Neural representation of bars, edges, and gratings in monkey primary afferents. *J. Neurophysiol., 46*, 1192–1203.

Phillips, J. R., Johansson, R. S., & Johnson, K. O. (1990). Representation of braille characters in human nerve fibers. *Exp. Brain Res., 81*, 589–592.

Phillips, J. R., Johansson, R. S., & Johnson, K. O. (1992). Responses of human mechanoreceptive afferents to embossed dot arrays scanned across fingerpad skin. *J. Neurosci., 12*, 827–839.

Phillips, J. R., Johnson, K. O., & Hsiao, S. S. (1988). Spatial pattern representation and transformation in monkey somatosensory cortex. *Proc. Natl. Acad. Sci. USA, 85*, 1317–1321.

Richmond, B. J., & Optican, L. M. (1987). Temporal encoding of two-dimensional patterns by single units in primate inferior temporal cortex. II. Quantification of response waveform. *J. Neurophysiol., 57*, 147–161.

Rosner, B. S. (1961). Neural factors limiting cutaneous spatiotemporal discrimination. In W. A. Rosenblith (Ed.), *Sensory communication* (pp. 725–737). Cambridge, MA: MIT Press.

Sejnowski, T. J. (1995). Pattern recognition: Time for a new neural code? *Nature, 376*, 21–22.

Shadlen, M. N., & Newsome, W. T. (1994). Noise, neural codes and cortical organization. *Curr. Opin. Neurobiol., 4*, 569–579.

Silva, L. R., Amitai, Y., and Connors, B. W. (1991). Intrinsic oscillations of neocortex generated by layer 5 pyramidal neurons. *Science, 251*, 432–435.

Simons, D. J. (1995). Neuronal integration in the somatosensory whisker / barrel cortex. In E. G. Jones and I. T. Diamond (Eds.), *Cerebral cortex* (Vol. 11, pp. 263–297). New York: Plenum Press.

Sinclair, R., & Burton, H. (1988). Responses from area 3b of somatosensory cortex to textured surfaces during active touch in primate. *Somatosens. Res., 5*, 283–310.

Sinclair, R. J., & Burton, H. (1991). Neuronal activity in the primary somatosensory cortex in monkeys (Macaca mulatta) during active touch of textured surface gratings: Responses to groove width, applied force, and velocity of motion. *J. Neurophysiol., 66*, 153–169.

Sinclair, R. J., Sathian, K., & Burton, H. (1991). Neuronal responses in ventroposterolateral nucleus of thalamus in monkeys (Macaca mulatta) during active touch of gratings. *Somatosens. Mot. Res., 8*, 293–300.

Steriade, M., McCormick, D. A., & Sejnowski, T. J. (1993). Thalamocortical oscillations in the sleeping and aroused brain. *Science, 262*, 679–685.

Swadlow, H. A. (1995). Influence of VPM afferents on putative inhibitory interneurons in S1 of the awake rabbit—Evidence from cross-correlation, mi-

crostimulation, and latencies to peripheral sensory stimulation. *J. Neurophysiol.*, *73*, 1584–1599.

Talbot, W. H., Darian-Smith, I., Kornhuber, H. H., & Mountcastle, V. B. (1968). The sense of flutter-vibration: Comparison of the human capacity with response patterns of mechanoreceptive afferents from the monkey hand. *J. Neurophysiol.*, *31*, 301–334.

Taylor, M. M., Lederman, S. J., & Gibson, R. H. (1973). Tactual perception of texture. In E. Carterette & M. Friedman (Eds.), *Handbook of perception* (Vol. 3, pp. 251–272). New York: Academic Press.

Theunissen, F., & Miller, J. P. (1995). Temporal encoding in nervous systems: A rigorous definition. *J. Comp. Neurosci.*, *2*, 149–162.

Tremblay, F., Ageranioti-Belanger, S. A., & Chapman, C. E. (1996). Cortical mechanisms underlying tactile discrimination in the monkey. I. Role of primary somatosensory cortex in passive texture discrimination. *J. Neurophysiol.*, *76*, 3382–3403.

Vega-Bermudez, F., Johnson, K. O., & Hsiao, S. S. (1991). Human tactile pattern recognition: Active versus passive touch, velocity effects, and patterns of confusion. *J. Neurophysiol.*, *65*, 531–546.

Viterbi, A. J. (1966). *Principles of coherent communication*. New York: McGraw-Hill.

Wang, X., Merzenich, M. M., Beitel, R., & Schreiner, C. E. (1995). Representation of a species-specific vocalization in the primary auditory cortex of the common marmoset: Temporal and spatial characteristics. *J. Neurophysiol.*, *74*, 2685–2706.

Welker, W. I. (1964). Analysis of sniffing of the albino rat. *Behaviour*, *22*, 223–244.

White, E. L., & Keller, A. (1987). Intrinsic circuitry involving the local axon collaterals of corticothalamic projection cells in mouse SmI cortex. *J. Comp. Neurol.*, *262*, 13–26.

Wilson, M. A., & Bower, J. M. (1989). The simulation of large-scale neural networks. In C. Koch and I. Segev (Eds.), *Methods in neuronal modeling: From synapses to networks* (pp. 291–333). Cambridge, MA: MIT Press.

Wise, S. P. (1993). Monkey motor cortex: Movements, muscles, motoneurons and metrics. *Trends. Neurosci.*, *16*, 46–49.

Yamamoto, T., Samejima, A., & Oka, H. (1988). Short latency activation of local circuit neurons in the cat somatosensory cortex. *Brain Res.*, *461*, 199–203.

Received August 1, 1996; accepted June 3, 1997.